

國立交通大學

電子物理系

碩士論文

層狀二類超導體在磁場中的傳輸行為

The transport properties of layered type II
superconductors in the magnetic field



研究生: 洪瑞甫

指導教授: 儒森斯坦 教授

中華民國九十八年十二月

層狀二類超導體在磁場中的傳輸行為

**The transport properties of layered type II
superconductors in the magnetic field**

研究生: 洪瑞甫

Student: Rui Fu Hung

指導教授: 儒森斯坦

Advisor: B. Rosenstein

國立交通大學



A Thesis

Submitted to Department of Electrophysics
National Chiao Tung University

In partial Fulfillment of the Requirement

For the Degree of

Master

In

Electrophysics

December 2009

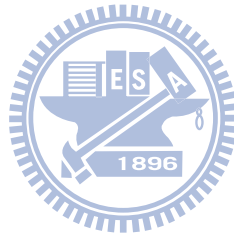
Hsinchu, Taiwan, ROC

層狀二類超導體在磁場中的傳輸行為

學生:洪瑞甫

指導教授: 儒森斯坦

國立交通大學電子物理系 (研究所) 碩士班



摘要

我利用 2 維 time - dependent Ginzburg - Landau 方程式來模擬計算出動態和靜態的 order parameters 和 超導電流。並由上述這兩個物理量來描述層狀二類超導體在磁場下(大於 H_{c1})所形成的 vortex 晶格結構。Vortex 晶格結構在乾淨超導體上有六角型的對稱性，然而當有外加電場進入超導體後，vortex 的晶格結構就會有微小的形變。另外所計算出的 I-V 曲線可以符合理論解析的結果。最近幾年具有奈米尺度的 pinning 陣列的超導體被制做出來並且受到注意，其中具有 Abrikosov 晶格對稱性的 pinning 陣列最備感興趣。由模擬計算出的動態 order parameter 可以看到在具有 pinning 陣列的超導體中的 vortex 流是由 interstitial vortex 所構成。而 I-V 曲線也會受到 pinning 陣列的影響，因為 vortices 會陷在 pinning centers 上而無法移動(如果 pinning force 小於 driving force)，如此一來由 vortex 移動所產生的能量損耗就可以減少。

The transport properties of layered type II superconductors in the magnetic field

Student: Rui Fu Hung

Advisor: Baruch Rosenstein

Institute of Electrophysics

National Chiao Tung University



Abstract

Static and dynamic distributions of the superconducting condensate order parameter and current density is studied by numerical simulation of the 2D time-dependent Ginzburg-Landau equations. They describe the vortex lattice in layered type II superconductors under magnetic fields above the lower critical field. In a clean superconductor the non-linear J-E characteristics were calculated and compared to existing analytic results. The Abrikosov lattice which is hexagonal in statics is deformed due to the electric field. The artificial pinning arrays on the nano scale were fabricated recently and are investigated for the most interesting case of the pinning superlattice commensurate with the Abrikosov lattice. The dynamical order parameter distribution shows that the vortex transport (flux flow) is conducted via diffusive motion of the so called interstitial vortices. The J-E characteristics are strongly influenced by the pinning, since the vortices are trapped on the pinning centers and thus the energy dissipation (Joule heat) inside the cores of the moving vortices is reduced.

ACKNOWLEDGMENT

首先要感謝我的指導教授，儒森斯坦老師，老師對學生總是細心指導，由淺入深、循序漸進的栽培我們。每當我遭遇瓶頸，老師也總是不吝嗇的指導我，教導我正面的研究態度，像我分享他的經驗和知識，在學短短兩年受益良多，老師諄諄教誨，使我銘感五內。接下來要感謝我的家人，家人總是默默的支持我，在物質上跟心靈上都給我很大的鼓勵，因為有家人的支持我才能順利的取得學位。最後要感謝在這兩年內給予我幫助的學長學姊與同學。



Contents

ABSTRSCT (CHINESE).....	i
ABSTRSCT (ENGLISH).....	ii
ACKNOWLEDGEMENT.....	iii
CONTENTS.....	iv
LIST OF FIGURES.....	vi
CHAPTER 1 Introduction.....	1
1.1 Superconductivity in strongly layered superconductors.....	1
1.1.1 <i>Type I and II superconductors in magnetic field</i>	2
1.1.2 <i>Layered structure and two dimensional superconductors</i>	4
1.1.3 <i>Vortex dynamics</i>	5
1.1.4 <i>Pinning in disordered superconductors</i>	6
1.2 Theoretical approaches to type II superconductivity.....	8
1.2.1 <i>London's approximation far from H_{c2}</i>	8
1.2.2 <i>Ginzburg-Landau approach far from H_{c1}</i>	8
1.3 Simulation methods and previous results for 2D GL for strongly type II supercon- ductors.....	10
1.3.1 <i>Monte Carlo simulation method. Static and thermodynamics properties</i> ..	10
1.3.2 <i>Molecular dynamics and the Langevin method</i>	11
CHAPTER 2 The relaxation method investigation of the static state of the Abrikosov lat- tice.....	13
2.1 2D Time Dependent Ginzburg Landau Model in continuum.....	13
2.1.1 <i>Free energy and the relaxation method</i>	13
2.1.2 <i>The dimensionless form</i>	14
2.2 Discrete TDGL on the hexagonal grid with Wilson link variables.....	16
2.2.1 <i>Hexagonal grid, site and link variables</i>	16
2.2.2 <i>Free energy on hexagonal lattice</i>	18
2.2.3 <i>Discretized TDGL equation</i>	19
2.2.4 <i>Boundary condition</i>	20
2.2.5 <i>Rectangular grid and boundary conduction</i>	21
2.2.6 <i>Free energy and TDGL equation in rectangular grid</i>	23
2.3 Simulation result and comparison of two grids.....	24
2.3.1 <i>Rectangular grid</i>	24
2.3.2 <i>Hexagonal grid</i>	25
CHAPTER 3 Model and simulation method for the vortex dynamics in clean system.....	32
3.1 Time Dependent Ginzburg-Landau theory in continuum.....	32
3.1.1 <i>Electric field in a mixed state superconductor and the flux flow</i>	32

3.1.2	<i>Dimensionless electric field and conductivity</i>	34
3.2	Discrete TDGL equation on rectangular grid.....	35
3.2.1	<i>Rectangular grid</i>	35
3.2.2	<i>Discretized supercurrent density</i>	36
3.3	Simulation result and discussion.....	37
3.3.1	<i>Parameters for YBCO</i>	37
3.3.2	<i>Superfluid density at flux flow</i>	38
3.3.3	<i>Definition of nonlinear conductivity and comparison of simulation with the analytic results</i>	39
CHAPTER 4	Vortex statics and dynamics in superconductor with periodic pinning	45
4.1	Time dependent Ginzburg-Landau theory with periodic pinning.....	45
4.2	Pinning distributions.....	46
4.3	Strong pinning array.....	47
4.3.1	<i>Superfluid density</i>	47
4.3.2	<i>Dynamics in the presence of pinning</i>	47
a.	<i>Interstitial vortices</i>	47
b.	<i>I-V curves</i>	49
4.4	Weaker pinning array.....	50
4.4.1	<i>Superfluid density</i>	52
4.4.2	<i>I-V curves</i>	52
CHAPTER 5	Conclusion	55
	Bibliography	57
	Appendix A	60
	Appendix B	62
	Appendix C	65
	Appendix D	69

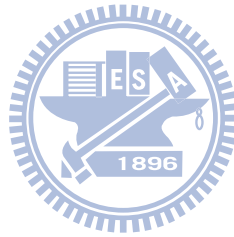


Table of list

Figure 1-1. Schematic magnetic phase diagram of a type II superconductor.....	3
Figure 1-2. Scanning superconducting quantum interference device (SQUID) microscopy (SSM)vortex imaging.[31].....	3
Figure 1-3. Parameters λ and ξ in S-N junction.....	4
Figure 1-4. Atomic structure in layered high Tc superconductor YBCO [25].....	5
Figure 1-5. The vortex flow.....	7
Figure 1-6. High-resolution scanning Hall probe microscopy Vortex configuration with periodic pinning[1].....	8
Figure 2-1. The unit vectors and vortex distance.....	17
Figure 2-2. Periodic boundary condition.....	21
Figure 2-3. The unit vectors and vortex distance.....	22
Figure 2-4. Average superfluid density as function of magnetic field(rectangular grid).....	25
Figure 2-5. Vortex structure ($b = 0.1$).....	26
Figure 2-6. Vortex structure ($b = 0.3$).....	27
Figure 2-7. Vortex structure ($b = 0.7$).....	28
Figure 2-8. Average superfluid density as function of magnetic field(hexagonal grid).....	29
Figure 2-9. Vortex structure ($b = 0.1$).....	30
Figure 2-10. Vortex structure ($b = 0.3$).....	31
Figure 2-11. Vortex structure ($b = 0.7$).....	31
Figure 3-1. Superfluid density with small electric field.....	39
Figure 3-2. Moving lattice with pinning	40
Figure 3-3. Comparison of simulated flux flow nonlinear conductivity with the analytic results.....	41
Figure 3-4. Comparison of simulated nonlinear j-E curve with analytic result.....	42
Figure 3-5. J-E curve for different ah (fix b).....	43
Figure 3-6. J-E curve for different ah (fix t)	44
Figure 4-1. Pinning distribution.....	47
Figure 4-2. Vortex structure with periodic pinning (pinning size = 4).....	48
Figure 4-3. Vortex structure with periodic pinning (pinning size = 9).....	48
Figure 4-4. Vortex structure with periodic pinning (pinning size = 16).....	49
Figure 4-5. Moving lattice with pinning.....	50
Figure 4-6. Comparison J-E curve for clean superconductors and superconductors with pinning array.....	51
Figure 4-7. Comparison of vortex lattices for clean superconductors and superconductors	

with pinning array.....52

Figure 4-8. Comparison of J - E curve for different strength of pinning potential ($u = 0$; $u = 0.5$; $u = 1$).....54



Chapter 1

Introduction

1.1 Superconductivity in strongly layered superconductors

Superconductivity is a remarkable property of metals and some other compounds at very low temperatures and generally signals Bose-Einstein condensation of pairs of electrons called Cooper pairs into a state in which dissipation processes are totally suppressed. On the macroscopic level this include two basic characteristic properties, zero electrical resistance and perfect diamagnetism. More quantitatively these phenomenon would happen when temperature is cooled below certain temperature T_c , which was called superconducting transition temperature (critical temperature). The Cooper pairs in superconducting metals (now termed "low temperature superconductors") are electron-electron bound states (more precisely resonances), with binding energy provided by a combined effect of the phonon exchange and the Pauli principle, overpowering the screened Coulomb repulsion. In more recent families of high T_c cuprates and pnictides the mechanism is most probably different (perhaps magnon mediated attraction), but unlike the metals for which the BCS theory is highly successful, the existing microscopic models are either too complicated or too infirm to be useful in studying mesoscopic or macroscopic phenomena or for applications.

The Cooper pairs are bosons and undergo Bose - Einstein condensation (BEC). Superconductivity therefore is a macroscopic quantum phenomenon (sometimes termed "mesoscopic"), since the phase ϕ (the Aharonov - Bohm or Josephson) of the Cooper pairs is coherent over very large distances. The BEC is purely a quantum mechanical phenomenon described by an

order parameter

$$\psi = \sqrt{n}e^{i\phi}, \quad (1.1)$$

where $n = |\psi|^2$ is Cooper pairs density. The phase In a homogeneous ground state this phase is arbitrary, since all values lead to the same total free energy.

According to the superconductor's response to external magnetic field, they can divided superconductors into two different classes: the type I superconductors and the type II superconductors.

1.1.1 Type I and II superconductors in magnetic field

For type-I superconductors, the external magnetic field almost does not penetrates interior of a superconducting sample. In other words, the magnetic field inside the sample is zero. This characteristics is called the "Meissner effect". The magnetization therefore M is $4\pi M = -H$. If the external field larger than a particular field H_c , called the critical field, the superconductivity would be destroyed. In contract, type-II superconductors have two critical fields H_{c1} and H_{c2} and two different states, show in Fig.1-1. When external field smaller than H_{c1} , the Meissner effect still exist and have no resistance. However, when external magnetic field between H_{c1} and H_{c2} , the small magnetic field would penetrate the superconductor sample and destroy superconducting state, thus both superconducting phase and normal phase in the superconductor sample, this states was called mixed state or the Shubnikov phase. When external magnetic is above H_{c2} , the magnetic field would break all the Cooper pairs, so that the sample's electronic state becomes normal .

In the mixed state of type II superconductors, the magnetic field enters the superconductors in the form of vortices, each carrying one unit of magnetic flux, $\Phi_0 = \frac{hc}{e^*}$, shown in Fig.1-2. The supercurrent flows around each vortex core which has essentially become normal state, and super current serve to screen out the magnetic filed outside the vortex. The physical explanation was pioneered by Abrikosov. The vortices repel each other with a long range force, usually, vortices arrange themselves in a form of hexagon to minimize mutual repulsion. The arrange of vortices similar to atomic lattice, therefore, it also be called Abrikosov lattice.

Two important length scales characterize a superconductor (shown in Fig.1-3 which de-

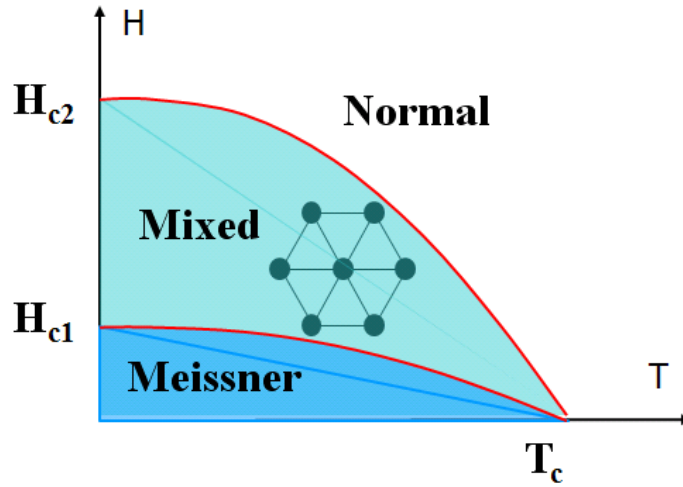


Figure 1-1: *Schematic magnetic phase diagram of a type II superconductor.* In the Meissner state, superconductivity remains perfect, while magnetic field is totally expelled. In the mixed state both the normal and the superconducting domains coexist. In the normal state, superconductivity is completely suppressed.

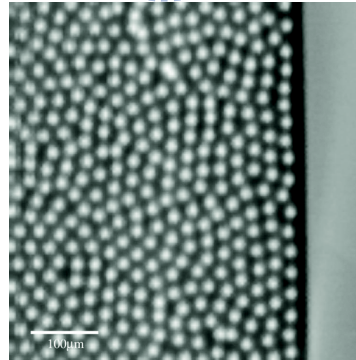
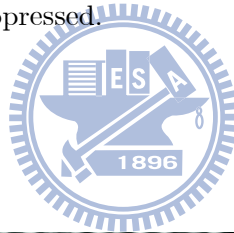


Figure 1-2: *Scanning superconducting quantum interference device (SQUID) microscopy (SSM) vortex imaging.*[31] Flux lattice (distances larger than penetration depth, that is the field is just above $H_{c1}(T)$, $H = 30mOe$) in near $\alpha - MoGe$ surface at $T = 4.2K$ is shown. White color corresponds to large magnetic field (vortices), while black color indicates superconducting domains between the vortices.

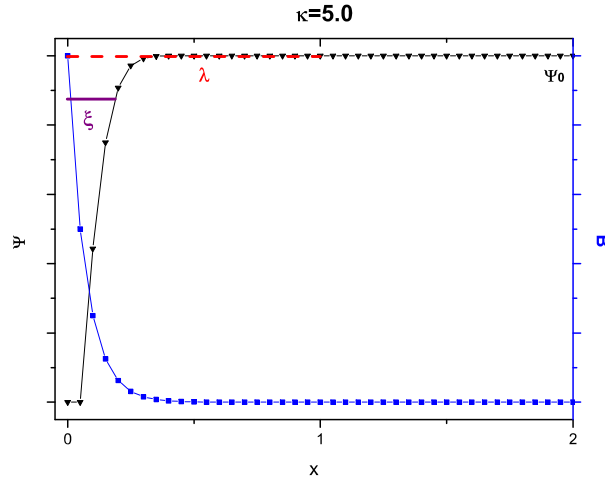


Figure 1-3: *Parameters ξ and λ in S-N junction.* This figure was simulated by using Carlo Method. Coherence length ξ has a Monte physical interpretation of the size of the Cooper pair bound state. Magnetic penetration depth λ is the distance inside the surface over which an external magnetic field is screened out to zero

scribes an S-N junction in narrow channel). Coherence length ξ has a physical interpretation of the size of the Cooper pair bound state, while the magnetic penetration depth λ is the distance inside the surface over which an external magnetic field is screened out to zero.

In conclusion, the type II superconductors not only can endure strong magnetic field but also have high critical temperature, thus, type II superconductors are quite important for both academic and industrial development.

1.1.2 Layered structure and two dimensional superconductors.

The crystalline structure of the type I and the type II superconductors is typically different. Usually type I superconductors are pure metal or their alloys and the Cooper pairs are bound in an s-wave state (have rotational symmetry). There are no important structural effects since the coherence length is much larger than the penetration depth. The type II superconductors typically are more complex. The most prominent representative class of a strongly type II materials, the high T_c cuprates are tetragonal, and all of them have one or more CuO_2 planes[23].

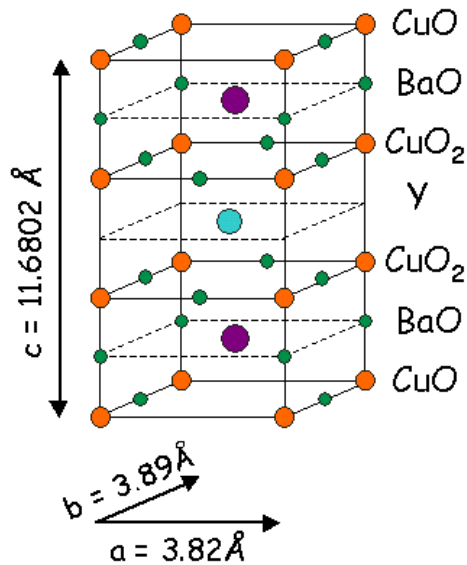


Figure 1-4: Atomic structure in layered high T_c superconductor $YBa_2Cu_3O_{7-\delta}$ [25]. Each unit cell has a CuO bilayer in which superconductivity resides.

see Fig.1-4. Other atoms like Bi , Y , Ba etc. separate the CuO_2 layers and provide charge carriers into CuO_2 planes. These layers are called charge reservoirs. The Cooper pairs move along CuO_2 planes and the properties for superconductivity become quasi-two dimension. Moreover, Cooper Pairs have the $d_{x^2-y^2}$ symmetry, namely are paired in an $l = 2$ state. The parameter γ , which is called the anisotropy parameter, is very large for $BSCCO$ and underdoped $YBCO$ (of order 50 or higher). These superconductors can be considered as two dimensional systems. Recently, layered superconductor $BSCCO$ become a major material for application like the THz wave generator.

1.1.3 Vortex dynamics

For type II superconductors, the dissipation of superconducting current is attribute to the magnetic quantized flux motion and it's transport properties have been derived form flux dynamic. For vortex is pushed by Lorentz force, thus, vortex move perpendicular to the electrical field, as show in Fig.1-5. For the phenomenologically of view, it's suitable to imagine a friction

force cause the dissipation

$$f_{dissipation} = -\eta \frac{d}{dt}x = -\eta v. \quad (1.2)$$

The over-damped dynamics results in motion of velocity with a constant velocity

$$-f_{dissipation} = \eta v = f_L = J \frac{\Phi_0}{c} \Rightarrow v = \frac{\Phi_0 J}{c\eta}. \quad (1.3)$$

Across the boundary of length L . It produces the flux change

$$\Delta\Phi = vBL\Delta t. \quad (1.4)$$

From the Maxwell equation,

$$\frac{1}{c} \frac{\Delta\Phi_0}{\Delta t} = V. \quad (1.5)$$

Substitute Eq.(1.4) into Eq.(1.5), the velocity of vortex is

$$v = \frac{cV}{BL} = \frac{cE}{B}. \quad (1.6)$$

The induce electronic field from the moving vortex is

$$E = \frac{v}{c}B = \frac{\Phi_0 JB}{c^2\eta}. \quad (1.7)$$

Note that the induce electric field is equal to the applied electric field. From the standpoint of the application of type II superconductors, it's important to understand how vortex dissipative process influence the I-V characteristic for type II superconductors.

1.1.4 Pinning in disordered superconductors

Disorder in superconductors originates from various sources. A partial list of intrinsic (namely existing in the material) defects includes point defects like the oxygen vacancies in cuprates, screw dislocation and twinning planes due to imperfections of the atomic structure, grain boundaries. On the mesoscopic scale the disorder would cause a short range pinning force which can hold the vortex. If the pinning forces are sufficiently strong and numerous, the vortex motion

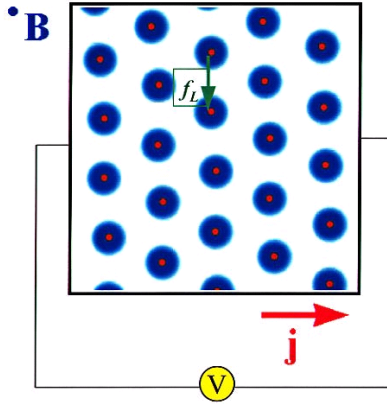


Figure 1-5: The *vortex flow*. The supercurrent flows in x direction. The magnetic field applied in z direction. The Lorentz force $f = q(v \times B) = J \frac{\Phi_0}{c}$, so Lorentz force is $-y$ direction, the vortex move perpendicularly to the supercurrent

can be arrested, so that the superconductor will restore the perfect conductor property. Physical quantities, such as, critical temperature, critical current, etc. are also affected by disorder. However, in technologically important materials critical current due to intrinsic pinning are not enough especially at high magnetic fields. One of the main reason is destructive competition of pinning centers, as demonstrated by the collective pinning theory [30, 29].

The type II superconductors with periodic artificial pinning have been studied in recent years, see Fig.1-6 . It was predicated theoretically [2] and confirmed experimentally [1, 3, 4] that when pinning centers are arranged into a periodic array commensurate with the Abrikosov lattice the critical current increases dramatically. The effect is maximized when the filling fraction is one, when one pinning center traps a single vortex. Additional vortices are "interstitial" and can be depinned easily thus significantly reducing the critical current [5]. Recently there have been an advance in the fabrication of the periodic arrays of pinning sites. The arrays with triangular, square, and rectangular geometries have been fabricated using either microholes or blind holes [1], magnetic dots [3] and columnar defects [4].

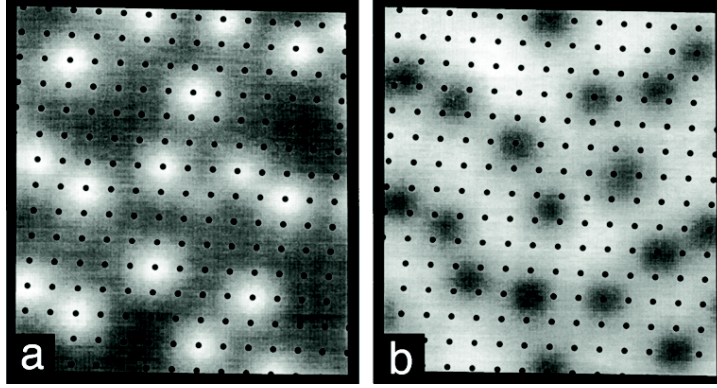


Figure 1-6: High-resolution scanning Hall probe microscopy *Vortex configuration with periodic pinning*[1]. Image for (a) $h = 1.916$ and (b) $h = 2.084$. the second matching field $h = 2$. The small dark circles are the positions of the holes. Below $h = 2$, the vacancies (white spots) all sit directly on holes; thus all vortices must as well. Above $h = 2$, the extra vortices (dark spots) sit on both hole and interstitial sites. Where $h = H/H_m$, $H_m = \Phi_0/a^2 = 5.913G$, $a = 1.87\mu m$ is pinning lattice constant. The sample investigated was a 100-nm-thick Nb film with 0.3-mm-diameter holes on square lattice

1.2 Theoretical approaches to type II superconductivity

1.2.1 London's approximation far from $H_{c2}(T)$

London theory is an earlier theory to phenomenologically describe Meissner effect and a superconducting state on the mesoscopic scale. This theory is very effective to describe electromagnetic properties of homogeneous superconductors [10] and is quite sufficient for the type I materials. It utilizes the fact that even in the mixed state at sufficiently low magnetic field most of the superconductor is in a superconducting state with maximal superfluid density $n_0 = |\psi_0|^2$. Neglecting small regions of vortex cores, one approximates $\psi = \psi_0$ and the only degree of freedom left is the magnetic field. The resulting linear (London's) equations replace the Maxwell equations, namely are the material electrodynamics of the superconductor.

1.2.2 Ginzburg-Landau approach far from $H_{c1}(T)$

Ginzburg-Landau (GL) theory which was proposed by Ginzburg and Landau in 1950 is a mean-field theory of the thermodynamic state. The most powerful feature is that it can be used to go beyond the original mean-field limit, so as to include the effect of thermal fluctuations. Thermal

fluctuation is not important for "low- T_c " superconductors; however, for high T_c superconductors is quite important, thermal fluctuation lead to many important phenomenon, such as flux flow, and vortex melting. GL theory had great success in describing intermediate-state phenomena of inhomogeneous superconductors.

Using the GL theory, Abrikosov showed that the two types of superconductors introduced in section 1.1 are distinguished by different value of a single parameter $\kappa = \lambda/\xi$ which is called Ginzburg-Landau parameter. Superconductors with $\kappa < 1/\sqrt{2}$ are type I superconductors, for $\kappa > 1/\sqrt{2}$ are type II superconductors. The interface energy (between normal state and superconductivity state, see Fig.) vanish when $\kappa = 1/\sqrt{2}$, which can be calculated exactly in the GL theory. For type I superconductors interface energy is positive. In other words, magnetic field would be eliminated inside superconductor samples. Therefore, type I superconductors only have two phases, superconductivity phase and normal phase. For type II superconductors, interface energy is negative; that is, external magnetic could enter superconductor samples and become mixed state and have a three phase magnetic phase diagram explaining Fig.1.

In strong magnetic fields magnetic envelopes of vortices overlap and field inside superconductor becomes homogeneous even in the mixed state. Not very far from $H_{c2}(T)$ the GL equation can be linearized and become similar to Schroedinger equation of an electron in homogeneous magnetic field. The energy spectrum become quantized [24].

$$E_n = \hbar\omega \left(n + \frac{1}{2} \right), \quad (1.8)$$

where $\omega = eB/m^*c$ is the cyclotron frequency, and $n = 0, 1, 2, \dots$ number the quantized Larmor orbits. As a result, the charged particles (Cooper pairs) can only occupy orbits with discrete energy values and one calls this these Landau levels. When $|H_{c2} - H| \ll H_{c2}$, the magnetic field is high enough, so that the solution belongs to the lowest Landau level (LLL). This is called the LLL approximation.

Using this approximation various static properties including effects of thermal fluctuations and disorder in vortex lattices were studied[8]. D.Li, B. Rosentein and V.Vinokur [14], provided a theory determining the glass transition in a disordered vortex system. For dynamical case, R. J. Troy and A. T. Dorsey studied the transport properties for type-II superconductors near

H_{c2} including electrical conductivity and transverse thermomagnetic effects (the Ettingshausen and Nernst effects), while D. Li, A. M. Malkin and B. Rosentein[15] studied the structure of the moving vortex lattice (clear system). They also contributions of high Landau levels.

1.3 Simulation methods and previous results for 2D GL for strongly type II superconductors

1.3.1 Monte Carlo simulation method. Static and thermodynamics properties

The Monte Carlo (MC) method is very popular in physics, engineering, economic, etc. In statistical physics, Metropolis algorithm is a most often used simulation method. MC simulations of phase transformation of type II superconductors in magnetic field using the phenomenological Ginzburg - Landau approach were performed over the last 15 years. Static thermal and magnetic properties of a clean 2D system in the presence of thermal fluctuations was simulated by Y. Kato and N. Nagaosa [11], who used the quasi-periodic boundary condition within the LLL approximation in Landau gauge. The finite size scaling of the algorithm was estimated to be N_s^2 (N_s is defined as the degrees of freedom). J. Hu and A. H. MacDonald[12] used the quasimomentum basis to speed up the simulation, so that the finite size scaling becomes N_s . Both J. Hu and A. H. MacDonald, Kato and Nagaosa, among others, found the first order phase transition from crystalline the liquid phase, by the double peak in probability of energy distribution $P(E)$

Disordered 2D system was first simulated only recently by M. S. Li and T. Nattermann[13]. They adopted the model of the disorder of the system with expanding the random Gaussian disorder in Hermite polynomials. They presented the results of the flux lattice melting transition and the behavior of the different correlation factor. They concluded that the phase transition from the curves of reduced temperature dependence of the structure factor splayed out near the melting temperature. No glass transition was found for the highest value of disorder considered the disorder parameter $\zeta = 0.01$. To my knowledge no simulations of the periodic arrays of pinning centers were performed within the framework of the GL model.

1.3.2 Molecular dynamics and the Langevin method

For the vortices can be seen as classical particles, therefore the Langevin equation is suitable to analyse vortex flow. The Langevin equation [17] is a mathematical model of dynamics of molecular system. This equation includes fluctuation and noise, so that it's good to represent molecular in real world. The Langevin equation as follows

$$\frac{dq_i}{d\tau} = -\frac{\partial S[q]}{\partial q_i} + \eta_i(\tau), \quad (1.9)$$

with correlation

$$\langle \eta(\tau) \eta^*(\tau') \rangle = \delta(\tau - \tau'). \quad (1.10)$$

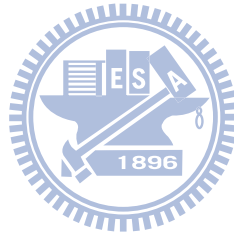
This nonlinear parabolic equation can be solved by following algorithms, Euler Method, Runge-Kutta Method, Crank-Nicholson method[18].

Although the MC method is economical to get the lowest free energy, however, the molecular relaxation process are also popular for studying vortex structure. Q. Du and M. D. Gunzburger[35] studied superconductivity including random pinning by finite-element method, Q. Du showed that pinning distribution influence the vortex structure and supercurrent flow around vortex. After few years, J. Deang, Q. Du and M. D. Gunzburger[20] added the thermal noise into the superconductors. As J. Deang showed the vortex hexagonal symmetric is broken by thermal noise. $U - \psi$ method was introduced by W. D. Gropp et al.[21], moreover this method is based on lattice gauge theory. This method is applicable to simulate magnetization system. W. D. Gropp showed the vortex relaxation process in large sample with random pinning. Kato, Enomoto, and Maekawa[27] studied the magnetization process and presented the hysteresis curve of magnetization.

For the point view of application, the nonlinear conductivity in type II superconductors is very important. M. Machida and H. Kaburaki[22] calculated I-V characteristics in type-II superconductors by using TDGL equation couple with Maxwell equation. After few years, D. Y. Vodolazov and F.M Peeters[19] used general TDGL equation to study moving vortex and find the critical velocity v_c , they also compared the I-V characteristic with vortex structure in different magnetic field. The Nernst effect in superconductors was studied by S. Mukerjee and

D. A. Huse[28], they used TDGL equation with thermal noise.

In this thesis, I using 2D TDGL equation to studied static and dynamic vortex system in strong layered superconductor, Forward-Difference method is used to solve TDGL equation in this simulation[36].In chapter 2, the static system was introduced, while in chapter 3, the dynamic system was studied. Both chapter 2 and chapter 3 study in clean superconductors. In chapter 4, the effect of periodic pinning were considered, both the static and dynamic case were studied in this chapter. The conclusion is in the last chapter.



Chapter 2

The relaxation method investigation of the static state of the Abrikosov lattice

2.1 2D Time Dependent Ginzburg Landau Model in continuum

2.1.1 Free energy and the relaxation method

In this work I use a numerical method to simulate the Time Dependent Ginzburg - Landau (TDGL) theory[32]. Here I first present a continuum version of the theory and in what follows "discretize" it on a grid, so that it is amenable to numerical simulation. A layered superconductor, in which the Cooper pairs move inside the Cu-O planes, is a quasi-two dimensional system. Therefore I consider the two-dimension TDGL equation

$$\frac{\gamma}{2} \frac{\hbar^2}{2m^*} \frac{\partial}{\partial t} \Psi = - \frac{\delta F[\Psi, \mathbf{A}]}{\delta \Psi^*}. \quad (2.1)$$

Here, Ψ is the (complex) order parameter, e^* and m^* are the Cooper pair's charge (considered positive) and effective mass. The inverse diffusion constant $\gamma/2$ is a real number, if relatively small Hall effect is neglected. I assume that the ratio $\kappa = \lambda/\xi \gg 1$. This means that magnetization is by a factor $1/\kappa^2$ smaller than the field and consequently (for magnetic field much larger than H_{c1}) $B \approx H$. The magnetic field $\mathbf{B} = \nabla \times \mathbf{A}$ therefore is homogeneous and constant. The

vector potential \mathbf{A} is chosen in symmetric gauge

$$\mathbf{A} = \frac{-1}{2}By\hat{i} + \frac{1}{2}Bx\hat{j}. \quad (2.2)$$

Ginzburg Landau free energy with constant magnetic field is

$$F[\Psi, \mathbf{A}] = \int d\mathbf{r} \frac{\hbar}{2m^*} |\mathbf{D}^2\Psi|^2 - \alpha T_c (1 - t') |\Psi|^2 + \frac{b'}{2} |\Psi|^4, \quad (2.3)$$

where $t' \equiv T/T_c$ is the dimensionless temperature, covariant derivatives are defined by $\mathbf{D} = \nabla - \frac{ie^*}{\hbar c} \mathbf{A}$, α and $b'(T)$ are phenomenological parameters which can be represented by coherence length ξ and penetration depth λ as $\alpha = \frac{\hbar^2}{2m^*\xi^2 T_c}$ and $b' = \frac{2\pi\hbar^2\lambda^2 e^{*2}}{\xi^2 c^2 m^{*2}}$. TDGL equation, therefore, can be written as

$$\frac{\gamma}{2} \frac{\hbar^2}{2m^*} \frac{\partial}{\partial t} \Psi = \frac{\hbar}{2m^*} \left(\nabla - \frac{ie^*}{\hbar c} \mathbf{A} \right)^2 \Psi + \alpha T_c (1 - t') \Psi - b' |\Psi|^2 \Psi. \quad (2.4)$$

Note that $\frac{\partial}{\partial t} \Psi$ is non-hermitian linear operator describing relaxation.

The density for Cooper pairs is $n_s = |\Psi|^2$, while the current density generally has two contributions $J = J_n + J_s$. $J_n = \sigma_0 E$ is the normal current density, while J_s is the supercurrent density

$$\begin{aligned} J_s &= \frac{\delta F[\Psi]}{\delta \mathbf{A}} = i \frac{e^* \hbar}{2m^*} (\Psi^* \mathbf{D} \Psi - \Psi \mathbf{D} \Psi^*) \\ &= i \frac{e^* \hbar}{2m^*} (\Psi^* \nabla \Psi - \Psi \nabla \Psi^*) + \frac{e^{*2}}{m_s c} |\Psi|^2 \mathbf{A}. \end{aligned} \quad (2.5)$$

2.1.2 The dimensionless form

It is convenient to use a dimensionless form of the TDGL equation. Sometimes, both the penetration depth λ_0 and the coherence length ξ_0 are used as units of length. In our simulation, the unit of length will be chosen to be ξ_0 : $\bar{x} = \frac{1}{\xi} x$; $\bar{y} = \frac{1}{\xi} y$. The unit of time characterizing the relaxation is $t_{GL} = \gamma \xi^2 / 2$, $\bar{t} = \frac{1}{t_{GL}} t$. The unit of magnetic field will be the upper critical field

H_{c2} , so that I use dimensionless quantities $b = \frac{1}{H_c} B \sqrt{2}$;

$$\mathbf{a} = \frac{1}{H_c \xi} \mathbf{A}; \quad \mathbf{a}_x = -\frac{b}{2} \bar{y}; \quad \mathbf{a}_y = \frac{b}{2} \bar{x}. \quad (2.6)$$

The maximal value of the order parameter (without magnetic field) $\Psi_0 = \sqrt{\alpha T_c / b}$ is the unit of order parameter: $\psi = \frac{1}{\sqrt{2} \Psi_0} \Psi$. In this units the TDGL equation, Eq.(2.4) is (detail please see Appendix A)

$$\frac{\partial}{\partial t} \psi = -\frac{\partial}{\partial \psi^*} f_{GL}. \quad (2.7)$$

Here f_{GL} is dimensionless free energy (dropping the bars from now on)

$$f_{GL} = \int d\mathbf{r} \psi^* \hat{H} \psi - a_h \psi^* \psi + \frac{1}{2} (\psi^* \psi)^2. \quad (2.8)$$

The dimensionless parameter,

$$a_h = \frac{1 - t' - b}{2}, \quad (2.9)$$

has a physical meaning of "distance" from the state normal-mixed state boundary in the H-T space. The operator

$$\hat{H} = -\frac{1}{2} \mathbf{D}^2 - \frac{b}{2}.$$

The dimensionless super current density is

$$j_s = J_s / J_{GL} = \frac{i}{2} (\psi^* \mathbf{D} \psi - \psi \mathbf{D} \psi^*) = \frac{i}{2} (\psi^* \nabla \psi - \psi \nabla \psi^*) + |\psi|^2 \mathbf{a} \quad (2.10)$$

,where the unit of current density is $J_{GL} = \frac{c H_{c2}}{2\pi \xi \kappa^2}$. The conductivity will be given in unit of

$$\sigma_0 = \frac{c^2 t_{GL}}{2\pi \lambda^2} = \frac{c^2 \gamma}{4\pi \kappa^2} \quad (2.11)$$

The rescaled model have two parameters: the temperature t , the magnetic field b . These two parameters determine the value of a_h .

2.2 Discrete TDGL on the hexagonal grid with Wilson link variables.

2.2.1 Hexagonal grid, site and link variables

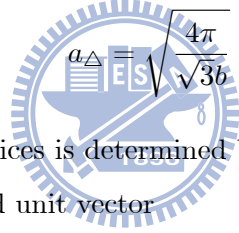
The points on the sample are described by two integers $\mathbf{n} = (n_1, n_2)$, where $n_1, n_2 = 1 \sim n_{\max}$. In order to simplify the simulation, the sample is following direction

$$\mathbf{r}_n = \frac{a_\Delta}{s} (n_1 \boldsymbol{\mu}_1 + n_2 \boldsymbol{\mu}_2) \quad (2.12)$$

with unit vectors of the Abrikosov lattice

$$\boldsymbol{\mu}_1 = (1, 0), \boldsymbol{\mu}_2 = \left(\frac{1}{2}, \frac{\sqrt{3}}{2} \right). \quad (2.13)$$

Here s is an integer and a_Δ is distance between vortex and vortex



$$a_\Delta \xi = \sqrt{\frac{4\pi}{\sqrt{3}B}} \quad (2.14)$$

The physical distance between vortices is determined by the flux quantization: $a_\Delta \xi = \sqrt{\frac{2\Phi_0}{\sqrt{3}B}}$. It is convenient to introduce a third unit vector

$$\boldsymbol{\mu}_3 = \boldsymbol{\mu}_2 - \boldsymbol{\mu}_1 = \left(\frac{-1}{2}, \frac{\sqrt{3}}{2} \right) \quad (2.15)$$

in order to represent the Laplace operator H (see Appendix). The unit vectors are show in Fig.2-1 for $s = 5$. The shape of grid is hexagonal (sometimes called "triangular"). It's more convenient to simulate a system under magnetic field by using the technique of link variables.

The method of the link variables describing electromagnetic field originated in the lattice gauge theory[33] used in simulations in particle physics. The general formula for link variable in our simulation is

$$U_{n_1, n_2}^\gamma = \exp(-i\theta_{n_1, n_2}^\gamma), \quad (2.16)$$

where $\theta_{n_1, n_2}^\gamma = \int_{\mathbf{n}}^{\mathbf{n}+\boldsymbol{\mu}^\gamma/s} \mathbf{a} \cdot d\mathbf{r}$ is the Aharonov - Baohm(A - B) phase, with \mathbf{a} is the dimensionless

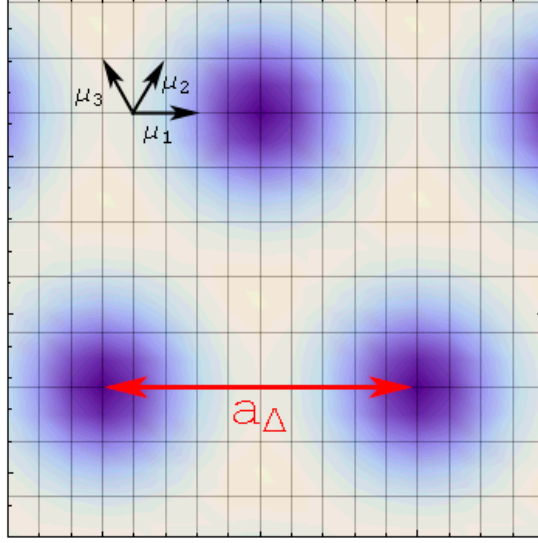


Figure 2-1: *The unit vectors and vortex distance.* a_Δ is the distance between vortex, where define in Eq.(2.14). μ_1, μ_2 and μ_3 are unit vectors, where define in Eq.(2.13) and Eq.(2.15)

vector potential, \mathbf{n} is the link's origin, while it ends at $\mathbf{n} + (a_\Delta/s) \boldsymbol{\mu}^\gamma$. The line integral is taken along the straight line. In order to simplify the calculation of the line integration, we define a parameter $0 < \alpha < 1$:

$$\frac{d}{d\alpha} \mathbf{r}^\gamma(\alpha) = \frac{a_\Delta}{s} \boldsymbol{\mu}_\gamma, \quad (2.17)$$

where $\gamma = 1, 2, 3$ and μ_γ is the unit vector which defined in Eq.(2.13,2.15).

The general formula for θ_{n_1, n_2}^γ is

$$\begin{aligned} \theta_{n_1, n_2}^\gamma &= \int_0^1 d\alpha \left\{ \left[\frac{d}{d\alpha} x^\gamma(\alpha) \right] a_x(\mathbf{r}^\gamma(\alpha)) + \left[\frac{d}{d\alpha} y^\gamma(\alpha) \right] a_y(\mathbf{r}^\gamma(\alpha)) \right\} \\ &= \frac{a_\Delta}{s} \int_0^1 d\alpha \{ \mu_x(\mathbf{r}^\gamma(\alpha)) + \mu_y a_y(\mathbf{r}^\gamma(\alpha)) \} \\ &= \frac{b a_\Delta}{2 s} \int_0^1 d\alpha \{ -\mu_x^\gamma y^\gamma(\alpha) + \mu_y^\gamma x^\gamma(\alpha) \}. \end{aligned} \quad (2.18)$$

Finally, the AB phase for each directions are (detail see Appendix D)

$$\theta_{n_1, n_2}^1 = -\frac{\sqrt{3}}{4} \frac{a_\Delta^2}{s^2} b n_2 \quad (2.19)$$

$$\theta_{n_1, n_2}^2 = \frac{\sqrt{3}}{4} \frac{a_\Delta^2}{s^2} b n_1$$

$$\theta_{n_1, n_2}^3 = \frac{\sqrt{3}}{4} \frac{a_\Delta^2}{s^2} b (n_1 + n_2), \quad (2.20)$$

where d is lattice distance. Substituting Eq.(2.14) into Eq.(2.19), we can get the following final formula

$$\theta_{n_1, n_2}^1 = -\frac{\pi}{s^2} n_2 \quad (2.21)$$

$$\theta_{n_1, n_2}^2 = \frac{\pi}{s^2} n_1$$

$$\theta_{n_1, n_2}^3 = \frac{\pi}{s^2} (n_1 + n_2).$$

2.2.2 Free energy on hexagonal lattice

The continuous first differential term $\frac{d}{dx} \psi(x)$ on the lattice can be naively defined (discretized) as

$$\sum_{n=1}^N \frac{\psi_{n+1}(x) - \psi_n(x)}{d}, \quad (2.22)$$

where d is distance between neighboring points. Unfortunately, the order parameter is a complex quantity which has the AB phase. To take into account the external magnetic field, link variable would be added into the formula. Therefore in magnetic field one makes the minimal substitution[21],

$$\frac{d}{dx} \psi(x) \rightarrow \sum_{n=1}^N \frac{U(x) \psi_{n+1}(x) - \psi_n(x)}{d}. \quad (2.23)$$

The free energy can be written as $f = f_{Grad} + f_{pot}$ where

$$\begin{aligned}
f_{grad} &= - \left(\frac{\sqrt{3}}{2} \right) \sum_{n_1, n_2=1}^{n_{\max}} \frac{2}{3} \psi_{n_1, n_2}^* \left\{ \begin{array}{l} U_{n_1, n_2}^1 \psi_{n_1+1, n_2} + (U_{n_1, n_2}^1)^* \psi_{n_1-1, n_2} + \\ U_{n_1, n_2}^2 \psi_{n_1, n_2+1} + (U_{n_1, n_2}^2)^* \psi_{n_1, n_2-1} + \\ U_{n_1, n_2}^3 \psi_{n_1-1, n_2+1} + (U_{n_1, n_2}^3)^* \psi_{n_1+1, n_2-1} \\ -6\psi_{n_1, n_2} \end{array} \right\} \quad (2.24) \\
f_{pot} &= \frac{\sqrt{3}}{2} \frac{a_{\Delta}^2}{s^2} \sum_{n_1, n_2=1}^{n_{\max}} \left[\frac{-(1-t')}{2} |\psi_{n_1, n_2}|^2 + \frac{1}{2} |\psi_{n_1, n_2}|^4 \right].
\end{aligned}$$

The factor $\sqrt{3}/2$ comes from the volume integration and the factor $3/2$ comes from the expression for the Laplace operator (see details in Appendix A). In Appendix B, I show that the discrete free energy matches the continuum free energy, Eq.(2.8). Discretized versions of various physical quantities could be derived from free energy. Examples include magnetization, heat capacity and the electric current density, see Chapter III.

2.2.3 Discretized TDGL equation

Substitute Eq.(2.24) into Eq.(2.1), the space part for TDGL equation is discretized, the formula is

$$\begin{aligned}
\frac{d}{dt} \psi_{n_1, n_2} &= \frac{1}{\sqrt{3}} \left[\begin{array}{l} U_{n_1, n_2}^1 \psi_{n_1+1, n_2} + (U_{n_1, n_2}^1)^* \psi_{n_1-1, n_2} + \\ U_{n_1, n_2}^2 \psi_{n_1, n_2+1} + (U_{n_1, n_2}^2)^* \psi_{n_1, n_2-1} + \\ U_{n_1, n_2}^3 \psi_{n_1-1, n_2+1} + (U_{n_1, n_2}^3)^* \psi_{n_1+1, n_2-1} \\ -6\psi_{n_1, n_2} \end{array} \right] \quad (2.25) \\
&+ \frac{\sqrt{3}}{2} \frac{a_{\Delta}^2}{s^2} \left[\frac{(1-t)}{2} \psi_{n_1, n_2} - |\psi_{n_1, n_2}|^2 \psi_{n_1, n_2} \right].
\end{aligned}$$

Then, I discretize time part $\frac{d}{dt} \psi_{n_1, n_2} = \frac{\psi_{n_1, n_2}(t+\Delta t) - \psi_{n_1, n_2}}{\Delta t}$. In order to simplify the equation, the $t + \Delta t$ terms put in left hand side, and t terms put in right hand side. Finally, The TDGL equation or the equation of motion of order parameters as following

$$\psi_{n_1, n_2}(t + \Delta t) = \psi_{n_1, n_2}(t) + \Delta t \mathcal{F}[\psi_{n_1, n_2}, U_{n_1, n_2}], \quad (2.26)$$

where

$$\begin{aligned}
\mathcal{F} [\psi_{n_1, n_2}, U_{n_1, n_2}] = & \quad (2.27) \\
& \frac{1}{\sqrt{3}} \left[\begin{array}{c} U_{n_1, n_2}^1 \psi_{n_1+1, n_2} + (U_{n_1, n_2}^1)^* \psi_{n_1-1, n_2} + \\ U_{n_1, n_2}^2 \psi_{n_1, n_2+1} + (U_{n_1, n_2}^2)^* \psi_{n_1, n_2-1} + \\ U_{n_1, n_2}^3 \psi_{n_1-1, n_2+1} + (U_{n_1, n_2}^3)^* \psi_{n_1+1, n_2-1} \\ - 6\psi_{n_1, n_2} \end{array} \right] + \\
& + \frac{\sqrt{3}}{2} \frac{a_\Delta^2}{s^2} \left[\frac{(1-t')}{2} \psi_{n_1, n_2} - |\psi_{n_1, n_2}|^2 \psi_{n_1, n_2} \right].
\end{aligned}$$

2.2.4 Boundary condition

I assume that the superconducting sample is large enough. In this case there is a well developed periodic vortex structure and the sample's boundaries very weakly influence the bulk. Consequently the periodic boundary condition (PBC), see Fig.2-2, is suitable for simulation of such a system. The PBC are a set of boundary conditions that are often used to simulate a large system by modelling a small part of it which is located far from its edge. The present system is more complicated due to local gauge invariance so that the magnetic translation group [34] should be considered. Periodicity is only up to a phase factor (AB phase) which is different for different locations and directions. The relation between the order parameters in the boundary as following

$$\begin{aligned}
\psi_{0, n_2} &= \exp \left[i \left(\frac{\pi}{s^2} L \right) \right] \psi_{L, n_2}; \psi_{L+1, n_2} = \left[i \left(\frac{\pi}{s^2} L \right) \right] \psi_{1, n_2}. \\
\psi_{n_1, 0} &= \exp \left[i \left(\frac{\pi}{s^2} L \right) \right] \psi_{n_1, L}; \psi_{n_1, L+1} = \left[i \left(\frac{\pi}{s^2} L \right) \right] \psi_{n_1, 1},
\end{aligned} \quad (2.28)$$

where

$$L = \frac{a_\Delta n_{\max}}{s}.$$

In order to simplify the boundary conditions, we let

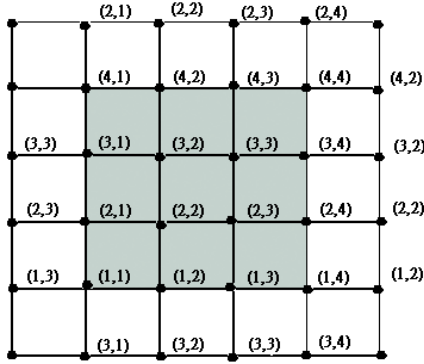


Figure 2-2: *Periodic boundary conditions.* The magnetic translations between the opposite along the boundaries on the grid are indicated. In actual computation four additional lines of "images" are used points. These are outside of the sample which is shown as a gray area.

$$L = 2Ns^2,$$

where N is a integer number, therefore, the boundary conditions become

$$\psi_{0,n_2} = \psi_{L,n_2}; \psi_{L+1,n_2} = \psi_{1,n_2}; \psi_{0,0} = \psi_{L,L}. \quad (2.29)$$

Discrete TDGL equation and simulation result in rectangular grid

2.2.5 Rectangular grid and boundary conduction

The points on the sample are also described by two integers(in unit of ξ) $\mathbf{n} = (n_1, n_2)$, where $n_1, n_2 = 1 \sim n_{\max}$. The sample is following direction

$$\mathbf{r}_n = \frac{a\Delta}{s} (n_1\boldsymbol{\mu}_1 + n_2\boldsymbol{\mu}_2), \quad (2.30)$$

with unit vector $\boldsymbol{\mu}_1 = (1, 0)$ and $\boldsymbol{\mu}_2 = \left(0, \frac{\sqrt{3}}{2}\right)$. The unit vectors show in Fig.2-3 as following and the shape of grid is rectangle.

The boundary condition for rectangle is periodic boundary condition with magnetic trans-

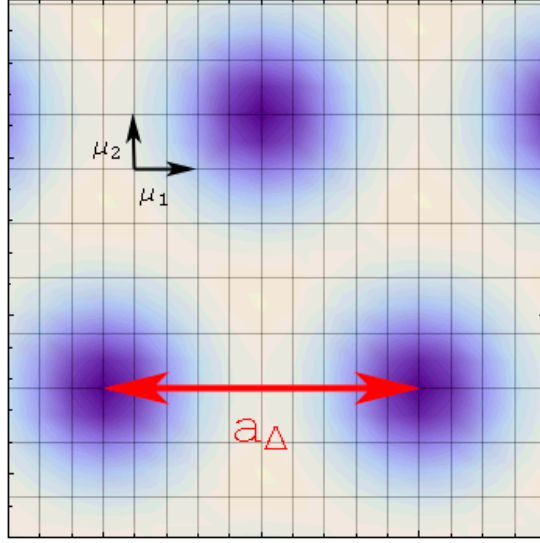
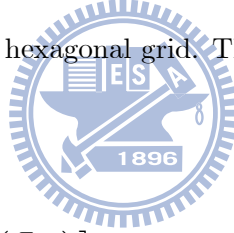


Figure 2-3: *The unit vectors and vortex distance.* a_{Δ} is the distance between vortex, where define in Eq.(2.14). μ_1, μ_2 are and unit vectors, where define in Eq.(2.13)

formation group which is similar as hexagonal grid. The relation between order parameters on the boundary is



$$\begin{aligned}\psi_{0,n_2} &= \exp\left[i\left(\frac{\pi}{s^2}L\right)\right]\psi_{L,n_2}; \psi_{L+1,n_2} = \left[i\left(\frac{\pi}{s^2}L\right)\right]\psi_{1,n_2} \\ \psi_{n_1,0} &= \exp\left[i\left(\frac{\pi}{s^2}L\right)\right]\psi_{n_1,L}; \psi_{n_1,0} = \left[i\left(\frac{\pi}{s^2}L\right)\right]\psi_{n_1,L+1}.\end{aligned}\quad (2.31)$$

Chose sample $L = 2Ns^2$, the boundary condition became following

$$\begin{aligned}\psi_{0,n_2} &= \psi_{L,n_2}; \psi_{L+1,n_2} = \psi_{1,n_2} \\ \psi_{n_1,0} &= \psi_{n_1,L}; \psi_{n_1,0} = \psi_{n_1,L+1}.\end{aligned}\quad (2.32)$$

In rectangle grid, link variables only have two directions, one for x direction another for y direction. The formula for link variable $U = \exp(-i\theta_{n_1,n_2}^\gamma)$, where $\gamma = 1, 2$. The must different of link variables between hexagonal grid and rectangle grid is θ_{n_1,n_2}^γ , for the link variable

represent the phase different between order parameters, in the other word, link variables are different in different shape of grid. The formula of θ_{n_1, n_2}^γ as following(detail see Appendix)

$$\begin{aligned}\theta_{n_1, n_2}^1 &= -\frac{\sqrt{3} a_\Delta^2}{4 s^2} b n_2 \\ \theta_{n_1, n_2}^2 &= \frac{\sqrt{3} a_\Delta^2}{4 s^2} b n_1.\end{aligned}\tag{2.33}$$

Although the formulas seem the same, but there are different link directions. Substituting Eq.(2.14) into Eq.(2.33), the final formulas are

$$\begin{aligned}\theta_{n_1, n_2}^1 &= -\frac{\pi}{s^2} n_2 \\ \theta_{n_1, n_2}^2 &= \frac{\pi}{s^2} n_1.\end{aligned}\tag{2.34}$$

2.2.6 Free energy and TDGL equation in rectangular grid

Similar as hexagonal grid, varied the differential terms with link variable $\frac{d}{dx} \psi(x) \rightarrow \sum_{n=1}^N \frac{U(x) \psi_{n+1}(x) - \psi_n(x)}{d}$.

The free energy $f = f_{\text{grad}} + f_{\text{pot}}$, where

$$\begin{aligned}f_{\text{grad}} &= -\left(\frac{\sqrt{3}}{2}\right) \sum_{n_1, n_2=1}^{n_{\text{max}}} \frac{1}{2} \psi_{n_1, n_2}^* \left\{ \begin{array}{l} U_{n_1, n_2}^1 \psi_{n_1+1, n_2} + (U_{n_1, n_2}^1)^* \psi_{n_1-1, n_2} + \\ \frac{4}{3} U_{n_1, n_2}^2 \psi_{n_1, n_2+1} + \frac{4}{3} (U_{n_1, n_2}^1)^* \psi_{n_1, n_2-1} \\ - \frac{14}{3} \psi_{n_1, n_2} \end{array} \right\} \\ f_{\text{pot}} &= \frac{\sqrt{3} a_\Delta^2}{2 s^2} \sum_{n_1, n_2=1}^{n_{\text{max}}} \left[\frac{-(1-t')}{2} |\psi_{n_1, n_2}|^2 + \frac{1}{2} |\psi_{n_1, n_2}|^4 \right].\end{aligned}\tag{2.35}$$

The factor 4/3 cause by the lattice distance for x direction(d) and y direction($\frac{\sqrt{3}}{2}d$) are different. And $\sqrt{3}/2$ come form volume integration.

Replace continuum free energy by discretized free energy in Eq.(4.3), the formula is

$$\begin{aligned} \frac{d}{dt}\psi_{n_1,n_2} = & \frac{\sqrt{3}}{4} \left[U_{n_1,n_2}^1 \psi_{n_1+1,n_2} + (U_{n_1,n_2}^1)^* \psi_{n_1-1,n_2} + \right. \\ & \left. \frac{4}{3} U_{n_1,n_2}^2 \psi_{n_1,n_2+1} + \frac{4}{3} (U_{n_1,n_2}^2)^* \psi_{n_1,n_2-1} - \frac{14}{3} \psi_{n_1,n_2} \right] \\ & + \frac{\sqrt{3}}{2} d^2 \left[\frac{(1-t)}{2} \psi_{n_1,n_2} - |\psi_{n_1,n_2}|^2 \psi_{n_1,n_2} \right]. \end{aligned} \quad (2.36)$$

Next, discrete time part

$$\frac{d}{dt}\psi_{n_1,n_2} = \frac{\psi_{n_1,n_2}(t+\Delta t) - \psi_{n_1,n_2}}{\Delta t}. \quad (2.37)$$

Similar as discretized TDGL equation in hexagonal grid, the TDGL equation can be written as equation of motion of order parameter finally. The formula is

$$\psi_{n_1,n_2}(t + \Delta t) = \psi_{n_1,n_2}(t) + \Delta t \mathcal{F}[\psi_{n_1,n_2}, U_{n_1,n_2}], \quad (2.38)$$

where

$$\begin{aligned} \mathcal{F}[\psi_{n_1,n_2}, U_{n_1,n_2}] = & \frac{\sqrt{3}}{4} \left[U_{n_1,n_2}^1 \psi_{n_1+1,n_2} + (U_{n_1,n_2}^1)^* \psi_{n_1-1,n_2} + \right. \\ & \left. \frac{4}{3} U_{n_1,n_2}^2 \psi_{n_1,n_2+1} + \frac{4}{3} (U_{n_1,n_2}^2)^* \psi_{n_1,n_2-1} - \frac{14}{3} \psi_{n_1,n_2} \right] + \\ & + \frac{\sqrt{3}}{2} d^2 \left[\frac{(1-t')}{2} \psi_{n_1,n_2} - |\psi_{n_1,n_2}|^2 \psi_{n_1,n_2} \right]. \end{aligned} \quad (2.39)$$

2.3 Simulation result and comparison of two grids.

2.3.1 Rectangular grid

The theory of $\langle \psi_{LLL}^2 \rangle$ was defined by D. Li, A. M. Malkin, and B. Rosensten[15], the definition as following

$$\langle \psi_{LLL}^2 \rangle = \frac{a_h}{\beta_A}, \quad (2.40)$$

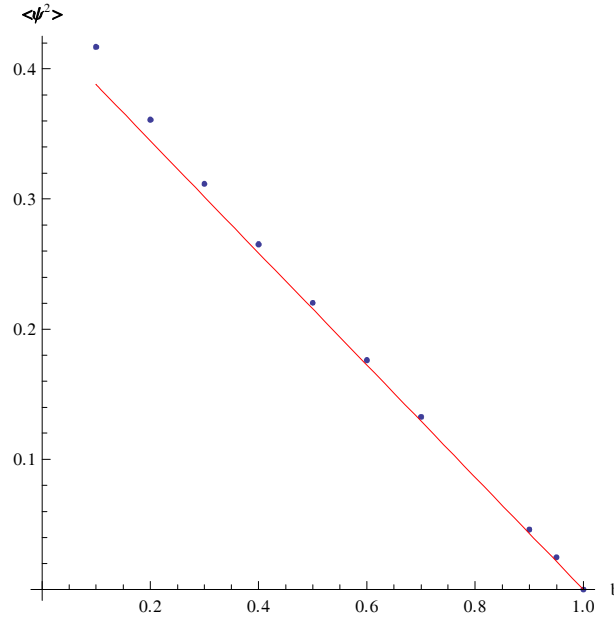


Figure 2-4: Average superfluid density $\langle |\psi|^2 \rangle$ as function of magnetic field (rectangular grid). The red line is values for the analytic expression Eq.(2.40). The blue points are simulation values for rectangular grid.

where $\beta_A = \frac{\langle \psi^4 \rangle}{\langle |\psi|^2 \rangle^2} = 1.16$ for hexagonal structure [32]. When the magnetic field is high enough ($a_h \ll 1$), the order parameters belong in LLL. Fig2-4 show relation between $\langle \psi^2 \rangle$ and b in $t = 0$,

The red line is theory value for Eq.(2.40), and the blue points are simulation values. When a_h become smaller, the $\langle |\psi|^2 \rangle$ for theory and simulation are closer. Superconductivity would totally break down when $a_h < 0$, since there is no condensation potential. The vortex structures in different magnetic fields are shown in following (Fig.2-5~Fig.2-7).

It's clearly that the distribution of vortex structure is hexagonal (vortex solid). The vortex density become larger when magnetic field become larger. Moreover, the values for $\langle \psi^2 \rangle$ become smaller. The Cooper pairs are broken by the magnetic field.

2.3.2 Hexagonal grid

Hexagonal grid is similar as Arbikosove lattice, the relation between average order parameters $\langle \psi^2 \rangle$ and magnetic field show in Fig.2-8

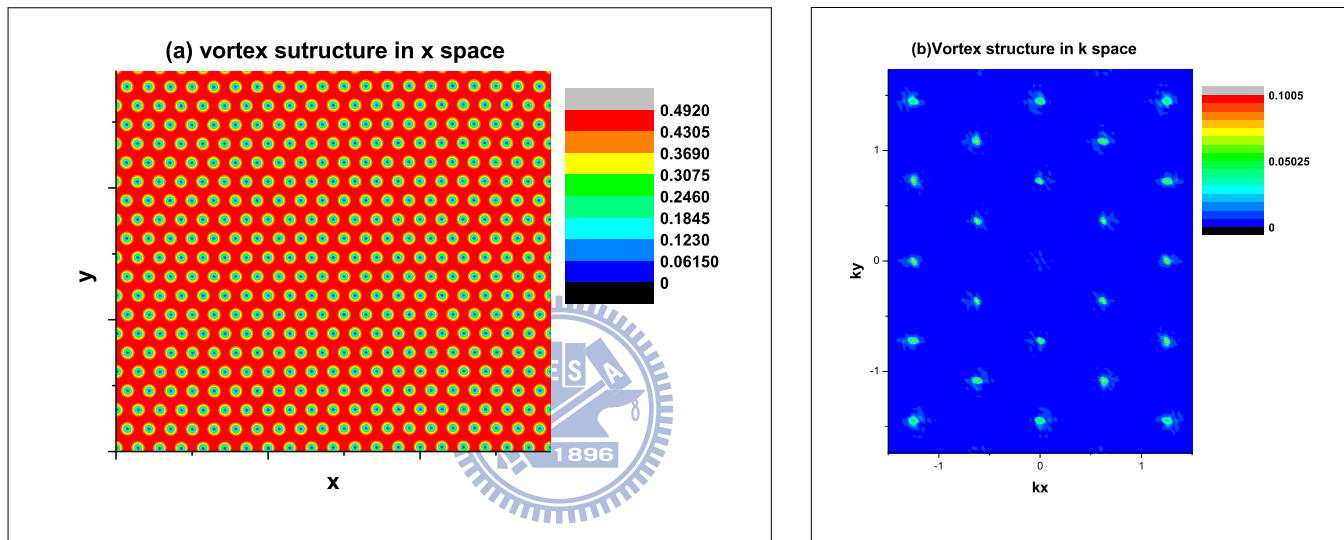


Figure 2-5: *Vortex structure*($b = 0.1$). The picture (a) is vortex lattice in real space, the vortex structure have the hexagonal symmetry. The picture (b) is the vortex spectrum in quasi-momentum space, the peaks are sharp and the peak distribution has hexagonal symmetry, therefore, this tell that the vortices in the solid phase.

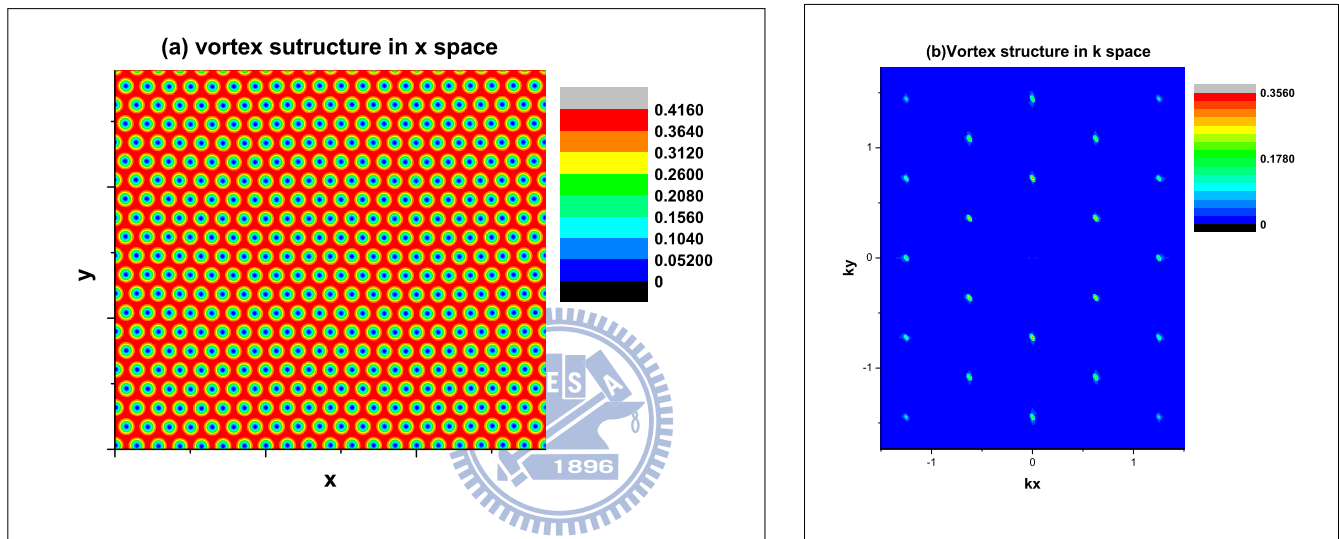


Figure 2-6: *Vortex structure*($b = 0.3$). Similar as Fig.2-5, the vortex lattice in real space (picture (a)) has hexagonal symmetry, and the peak distribution for the vortex spectrum (picture (b)) still has hexagonal symmetry. The order parameters ($|\psi|^2$) in large magnetic field ($b = 0.3$) are smaller than small magnetic field ($b = 0.7$), because of the Cooper pairs are broke by the magnetic field

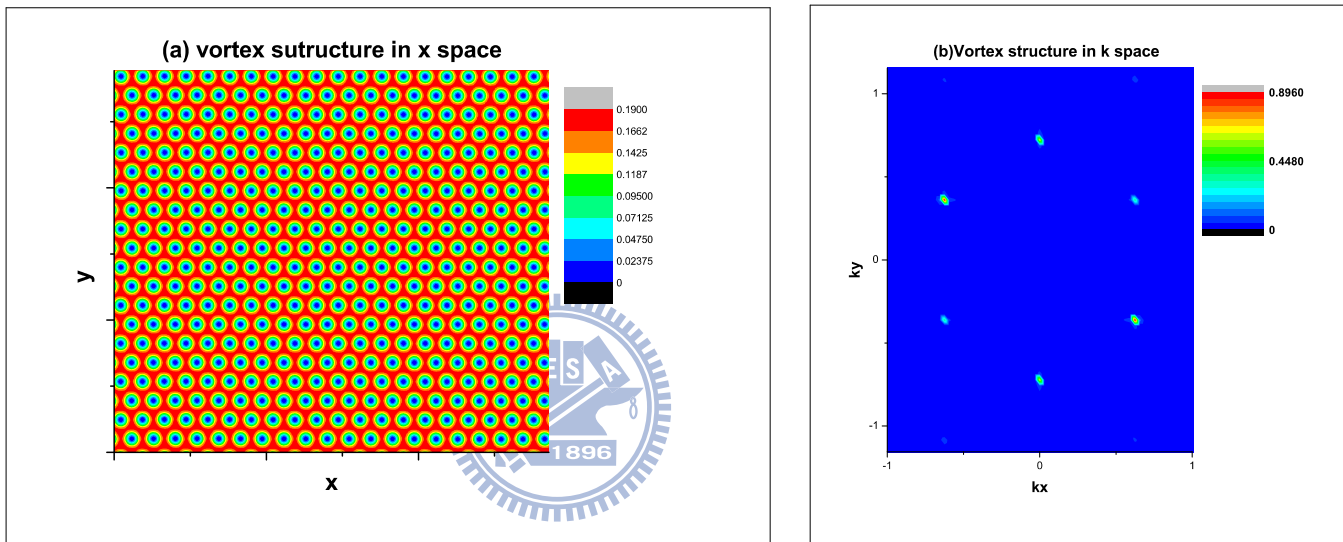


Figure 2-7: *Vortex structure*($b = 0.7$). Similar as Fig.2-5, the vortex lattice in real space(picture(a)) has hexagonal symmetry, and the peak distribution for the vortex spectrum(picture(b)) still has hexagonal symmetry. The order parameters($|\psi|^2$) in large magnetic field($b = 0.7$) are samller than small magnetic field($b = 0.3$).

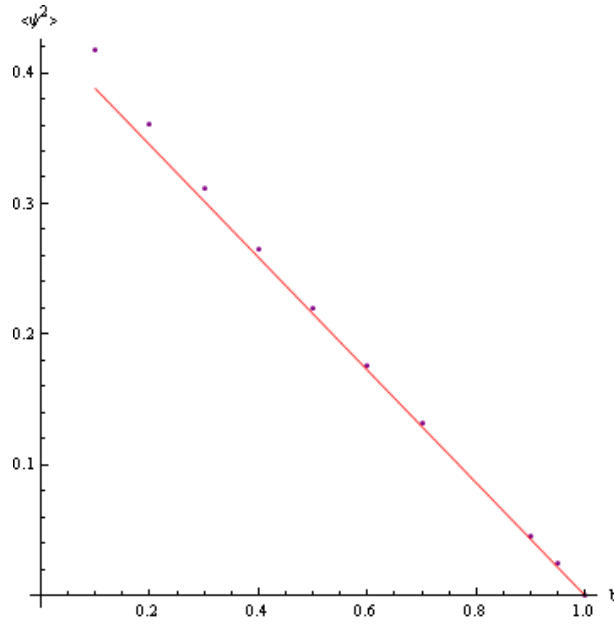


Figure 2-8: *Average superfluid density $\langle |\psi|^2 \rangle$ as function of magnetic field(hexagonal grid).* The red line is values for the analytic expression Eq.(2.40). The purple points are simulation values in hexagonal grid, and almost the same as values for rectangular grid.

The red line is theory value where come form Eq.(2.40), the purple points are simulation value. The value for $\langle \psi^2 \rangle$ rectangular grid and for hexagonal grid are almost the same. The vortex structure in different magnetic field as shown in the following, see Fig.2-8~Fig.2-10. Similar as vortex structure on rectangular grid, the vortex structure are also has hexagonal symmetry. The hexagonal grid is more symmetric than rectangular grid, however, the vortex lattice structure on the rectangular grid is more beautiful than on the hexagonal grid, since the relaxation time for hexagonal grid is larger than rectangular grid.

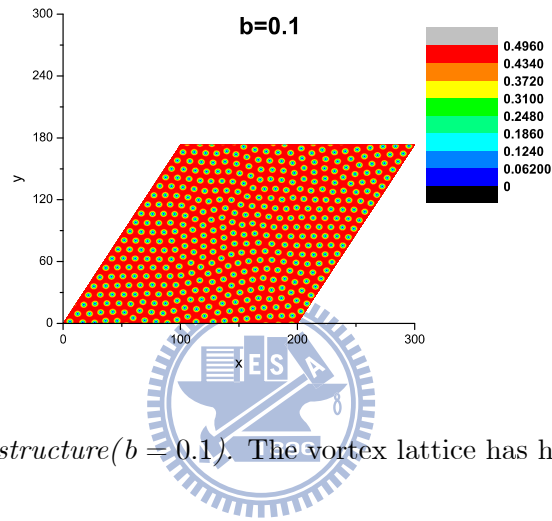


Figure 2-9: *Vortex structure*($b = 0.1$). The vortex lattice has hexagonal symmetry.

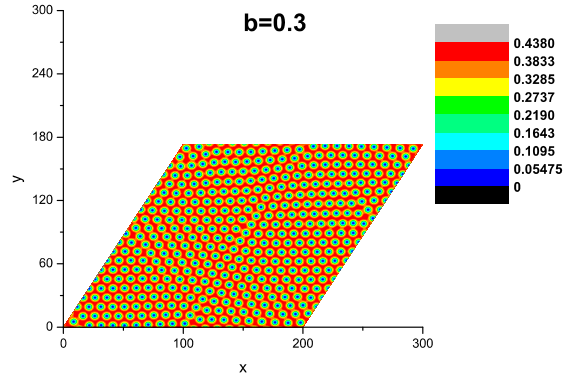


Figure 2-10: *Vortex structure*($b = 0.3$). The vortex lattice also has hexagonal symmetry.

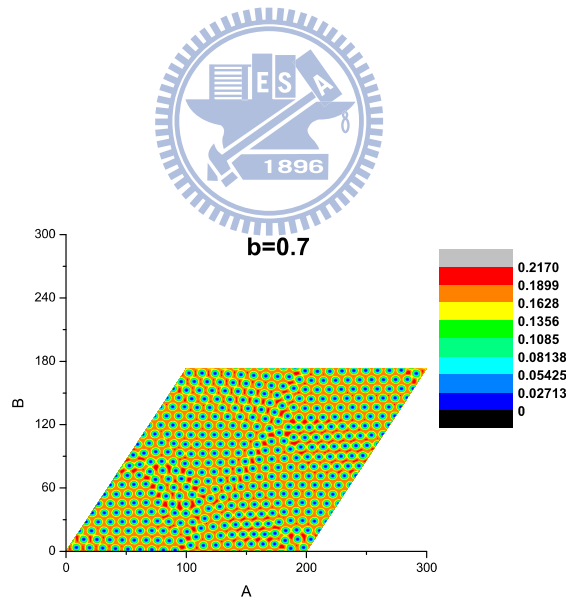


Figure 2-11: *Vortex structure*($b = 0.7$). The vortex lattice also has hexagonal symmetry, and the values of order parameters become smaller, the Cooper pairs are broken by the magnetic field.

Chapter 3

Model and simulation method for the vortex dynamics in clean system

3.1 Time Dependent Ginzburg-Landau theory in continuum

3.1.1 Electric field in a mixed state superconductor and the flux flow

In previous chapter I discussed the static vortex system. The system would eventually relax to a lowest free energy state. The relaxation dynamics was not realistic in a sense that effects of the electric field were neglected (which is not essential for the static properties of the system since the final state is the same). In this chapter I start to consider dynamics of a type II superconductor in external magnetic and electric fields. When the electric field applied to the system, it acts on vortices as an external force. Consequently the TDGL equation should be modified as following

$$\frac{\gamma}{2} \frac{\hbar^2}{2m^*} \left(\frac{\partial}{\partial t} + \frac{ie^*}{\hbar} \Phi \right) \Psi = - \frac{\delta F[\Psi, \mathbf{A}]}{\delta \Psi^*}, \quad (3.1)$$

where the free energy was defined in Eq.(chapter II). Here, Φ is an electric potential and γ is the inverse diffusion constant. The electric field is $\mathbf{E} = -\nabla\Phi - \frac{1}{c} \frac{\partial \mathbf{A}}{\partial t}$, while the magnetic field is given by $\mathbf{B} = \nabla \times \mathbf{A}$. The TDGL equation is invariant under the gauge transformation

$$\begin{aligned}
\Psi &= \Psi \exp\left(-i\frac{e^*}{\hbar c}\chi\right); \\
A &= A + \nabla\chi; \\
\Phi &= \Phi - \frac{1}{c}\frac{\partial\chi}{\partial t},
\end{aligned} \tag{3.2}$$

where χ is an arbitrary function of space and time. Choosing the zero scalar potential gauge is convenient for the simulations which follow:

$$\begin{aligned}
\Phi &= 0 \\
\mathbf{A} &= \frac{-1}{2}Bx\hat{i} + \left(\frac{1}{2}By - cEt\right)\hat{j}.
\end{aligned} \tag{3.3}$$

Here both magnetic and electric fields are assumed to be constant. Dynamics of electromagnetic field should in principle also taken into account by the Maxwell equations. However as explained in chapter II, for strongly type II superconductors magnetization is of order $1/\kappa^2$ and hence negligible. Vortices overlap and their magnetic fields become homogeneous. Electric fields in the flux flow state are also homogeneous (except at very low values in the presence of pinning, see chapter IV) and their dynamics can be neglected as well except for the normal conductivity

$$J = \sigma_n E. \tag{3.4}$$

Substituting the free energy $F[\Psi, A]$ of Eq.(chapter II) into equation, the TDGL equation becomes

$$\frac{\gamma}{2} \frac{\hbar^2}{2m^*} \frac{\partial}{\partial t} \Psi = \frac{\hbar}{2m^*} \left(\nabla - \frac{ie}{\hbar c} \mathbf{A} \right)^2 \Psi + \alpha T_c (1 - t') \Psi - b' |\Psi|^2 \Psi. \tag{3.5}$$

The formula is formally identical to the static TDGL equation, however the vector potential now contains a time dependent part. The time derivative term is purely dissipative (relaxational) and carries an implicit the information about the vortex velocity. When vortices move faster the frequency of phase change becomes larger, and finally, the vortex structure would break down and the order parameter goes to zero. Because of the energy dissipation, resistance of

type II superconductors is not zero. The formula for supercurrent density is the same as in the static case.

$$\mathbf{J}_s = i \frac{e^* \hbar}{2m^*} (\Psi^* \nabla \Psi - \Psi \nabla \Psi^*) + \frac{e^{*2}}{m_s c} |\Psi|^2 \mathbf{A}. \quad (3.6)$$

Note that the supercurrent density is also invariant under gauge transformation.

3.1.2 Dimensionless electric field and conductivity

Using the same units as in static case, ξ, t_{GL} , the derived units of electric field is $E_{GL} = \frac{ct_{GL}}{\xi} H_{c2} = \frac{c\gamma\xi}{2} H_{c2}$. In *YBCO* this field is very large. Therefore the dimensionless electric field will be defined as

$$\epsilon = E/E_{GL}. \quad (3.7)$$

Consequently the dimensionless vector potential is

$$\mathbf{a} = \left(\frac{-1}{2} by, \frac{1}{2} bx - \epsilon t \right), \quad (3.8)$$

here x and y in unit of ξ , and t in unit of t_{GL} . The velocity of vortices, which in physical units is $\mathbf{V} = c\mathbf{E}/\mathbf{B}$, in dimensionless units reads:

$$v = V \frac{t_{GL}}{\xi} = \frac{cE}{B} \frac{t_{GL}}{\xi} = \frac{E}{E_{GL}} * \frac{H_{c2}}{B} = \frac{\epsilon}{b}.$$

The dimensionless TDGL equation takes a form

$$\frac{\partial}{\partial t} \psi = \hat{H} \psi - a_h \psi + (\psi^* \psi) \psi, \quad (3.9)$$

where $\hat{H} = -\frac{1}{2} \mathbf{D}^2 - \frac{b}{2}$,

$$a_h = \frac{1 - t' - b}{2}, \quad (3.10)$$

and the dimensionless supercurrent density

$$j_s = \frac{i}{2} (\psi^* \nabla \psi - \psi \nabla \psi^*) + |\psi|^2 \mathbf{a}, \quad (3.11)$$

are the same as in the static case, with the only difference being the electric field term in vector potential, Eq.(3.8).

3.2 Discrete TDGL equation on rectangular grid

3.2.1 Rectangular grid

The discretized version of the dynamic TDGL equation is similar to the statistic one, the only difference being the link variables for the gauge field. The link variable

$$U_{n_1, n_2}^\gamma = \exp(-i\theta_{n_1, n_2}^\gamma), \quad (3.12)$$

where AB phase

$$\theta_{n_1, n_2}^\gamma = d \int_0^1 \{d\alpha \mu_x a_x(\mathbf{r}^\gamma(\alpha)) + \mu_y a_y(\mathbf{r}^\gamma(\alpha))\}. \quad (3.13)$$

For the nonequilibrium system, the link variables change with time, the link variables in μ_1 and μ_2 directions are

$$\begin{aligned} \theta_{n_1, n_2}^1 &= -\frac{1}{2} \frac{a_\Delta}{s} by \\ \theta_{n_1, n_2}^2 &= \frac{\sqrt{3}}{4} \frac{a_\Delta}{s} bx - \frac{\sqrt{3}}{2} \frac{a_\Delta}{s} ct, \end{aligned} \quad (3.14)$$

where the distance between vortex $a_\Delta = \sqrt{\frac{4\pi}{\sqrt{3}b}}$, $x = \frac{a_\Delta}{s} n$, $y = \frac{\sqrt{3}}{2} \frac{a_\Delta}{s} n_2$. Substitute a_Δ , x and y into Eq.(3.14),

$$\begin{aligned} \theta_{n_1, n_2}^1 &= -\frac{\pi}{s^2} n_2 \\ \theta_{n_1, n_2}^2 &= \frac{\pi}{s^2} n_1 - \frac{\sqrt{3}}{2} \frac{a_\Delta}{s} ct. \end{aligned} \quad (3.15)$$

The discretized dynamic TDGL equation is similar as static case, the only difference is the link variables. The formula show as following

$$\begin{aligned} \frac{d}{dt}\psi_{n_1, n_2} = & \frac{\sqrt{3}}{4} \left[U_{n_1, n_2}^1 \psi_{n_1+1, n_2} + (U_{n_1, n_2}^1)^* \psi_{n_1-1, n_2} + \right. \\ & \left. \frac{4}{3} U_{n_1, n_2}^2 \psi_{n_1, n_2+1} + \frac{4}{3} (U_{n_1, n_2}^2)^* \psi_{n_1, n_2-1} - \frac{14}{3} \psi_{n_1, n_2} \right] \\ & + \frac{\sqrt{3}}{2} d^2 \left[\frac{(1-t)}{2} \psi_{n_1, n_2} - |\psi_{n_1, n_2}|^2 \psi_{n_1, n_2} \right]. \end{aligned} \quad (3.16)$$

3.2.2 Discretized supercurrent density

The the definition of supercurrent density

$$j_\mu = \frac{\delta f_{\text{grad}}}{\delta a_\mu}, \quad (3.17)$$

where $\mu = 1, 2$, f is the dimensionless free energy. The supercurrent density in x and y direction as following

$$\begin{aligned} j_x &= \frac{i}{2 \frac{a_\Delta}{s}} (U_{n_1, n_2}^1 \psi_{n_1, n_2}^* \psi_{n_1+1, n_2} - c.c) \\ j_y &= \frac{i}{2 \left(\frac{\sqrt{3} a_\Delta}{2 s} \right)} (U_{n_1, n_2}^2 \psi_{n_1, n_2}^* \psi_{n_1, n_2+1} - c.c). \end{aligned} \quad (3.18)$$

Next, I expand discretized supercurrent density formula to get continuum formula. Use Taylor expansion to expand link variables U_{n_1, n_2}^γ and order parameters ψ_{n_1, n_2} ,

$$\begin{aligned} U_{n_1, n_2}^\gamma &= \exp(-i\theta_{n_1, n_2}^\gamma) \simeq 1 - i\theta_{n_1, n_2}^\gamma \\ \psi_{n_1+1, n_2} &= \psi + \frac{a_\Delta}{s} \frac{\partial}{\partial x} \psi \\ \psi_{n_1, n_2+1} &= \psi + \frac{3 a_\Delta}{2 s} \frac{\partial}{\partial y} \psi, \end{aligned} \quad (3.19)$$

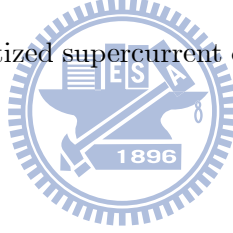
where $\gamma = 1, 2$, both θ_{n_1, n_2}^1 and θ_{n_1, n_2}^2 were defined in Eq.(3.14). The discretized supercurrent density in x direction can be write as

$$\begin{aligned}
j_x &= \frac{i}{2\left(\frac{a_\Delta}{s}\right)} \left[(1 - i\theta_{n_1, n_2}^1) \psi^* \left(\psi + \frac{a_\Delta}{s} \frac{\partial}{\partial x} \psi \right) - \right. \\
&\quad \left. (1 + i\theta_{n_1, n_2}^1) \psi_{n_1, n_2} \left(\psi_{n_1, n_2}^* + \frac{a_\Delta}{s} \frac{\partial}{\partial x} \psi_{n_1, n_2}^* \right) \right] \\
&= \frac{i}{2} \left(\psi_{n_1, n_2}^* \frac{\partial}{\partial x} \psi_{n_1, n_2} - \psi_{n_1, n_2} \frac{\partial}{\partial x} \psi_{n_1, n_2}^* \right) + \frac{s}{a_\Delta} \theta_{n_1, n_2}^1 |\psi_{n_1, n_2}|^2 \\
&= \frac{i}{2} \left(\psi_{n_1, n_2}^* \frac{\partial}{\partial x} \psi_{n_1, n_2} - \psi_{n_1, n_2} \frac{\partial}{\partial x} \psi_{n_1, n_2}^* \right) + a_x |\psi_{n_1, n_2}|^2.
\end{aligned}$$

Similarly, The discretized supercurrent density in y direction

$$\begin{aligned}
j_y &= \frac{i}{2\left(\frac{\sqrt{3} a_\Delta}{2s}\right)} \left[(1 - i\theta_{n_1, n_2}^1) \psi_{n_1, n_2}^* \left(\psi_{n_1, n_2} + \frac{\sqrt{3} a_\Delta}{2s} \frac{\partial}{\partial y} \psi_{n_1, n_2} \right) - \right. \\
&\quad \left. (1 + i\theta_{n_1, n_2}^1) \psi_{n_1, n_2} \left(\psi_{n_1, n_2}^* + \frac{\sqrt{3} a_\Delta}{2s} \frac{\partial}{\partial y} \psi_{n_1, n_2}^* \right) \right] \\
&= \frac{i}{2} \left(\psi_{n_1, n_2}^* \frac{\partial}{\partial y} \psi_{n_1, n_2} - \psi_{n_1, n_2} \frac{\partial}{\partial y} \psi_{n_1, n_2}^* \right) + \frac{2s}{\sqrt{3} a_\Delta} \theta_{n_1, n_2}^1 |\psi_{n_1, n_2}|^2 \\
&= \frac{i}{2} \left(\psi_{n_1, n_2}^* \frac{\partial}{\partial y} \psi_{n_1, n_2} - \psi_{n_1, n_2} \frac{\partial}{\partial y} \psi_{n_1, n_2}^* \right) + a_y |\psi_{n_1, n_2}|^2.
\end{aligned}$$

Both the continuum limit for discretized supercurrent density in x and y direction are the same as continuum formulas Eq.(3.11).



3.3 Simulation result and discussion

3.3.1 Parameters for $YBCO$

To the following parameters of $YBCO$ sample as used. $T_c = 100K$, $H_{c2} = 140T$, $m^* = 2m_e$.

The coherence length and the penetration depth:

$$\begin{aligned}
\xi &= \frac{\hbar}{(2m^* \alpha T_c)^{1/2}} = 1.53nm \rightarrow \alpha = \frac{\hbar^2}{(2m^* T_c \xi^2)} = 0.94, \\
\lambda &= \frac{c}{2e^*} \sqrt{\frac{m^* b'}{\pi \alpha T_c}} = 140nm \rightarrow b' = \frac{4\pi \alpha T_c e^{*2} \lambda^2}{c^2 m^*} = 1.8 * 10^{-35} \frac{Cm^5 G}{s^2}.
\end{aligned} \tag{3.20}$$

The Lattice spacing is

$$\xi a_{\Delta} = \sqrt{\frac{2\Phi_0}{\sqrt{3}B}} = \sqrt{\frac{2\Phi_0}{\sqrt{3}Hc_2}} b^{-1/2} = 4.1nm b^{-1/2}; \quad a_{\Delta} = \sqrt{\frac{4\pi}{\sqrt{3}b}}. \quad (3.21)$$

magnetic field $b = 0.1$ in this simulation $a_{\Delta}\xi \simeq 13nm$. The unit of time is:

$$\sigma_n = \frac{c^2\gamma}{8\pi\kappa^2} = 5 * 10^3 ohm^{-1}cm^{-1} = \frac{5}{1.1} * 10^3 * 10^{12} sec^{-1} = 4.545 * 10^{15}$$

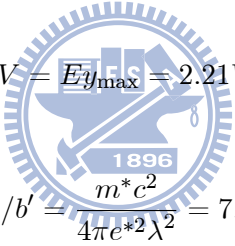
$$\rightarrow \gamma = \frac{8\pi\kappa^2}{c^2}\sigma_n = \frac{8\pi\left(\frac{140}{1.53}\right)^2(4.545*10^{15})}{(3*10^{10})^2} = 1.06 s/cm^2$$

$$t_{GL} = \gamma\xi^2/2 = 1.24 * 10^{-14}s, \quad (3.22)$$

and unit of electric field

$$E_{GL} = Hc_2 \frac{\xi}{ct_{GL}} = 578G^{1/2}Cm^{-1/2}Sec^{-1} = 1.7 * 10^5 Vot/Cm \quad (3.23)$$

For sample size $y_{\max} = 10 * 13 * 10^{-7}Cm = 1.3 * 10^{-5}Cm$, voltage is

$$V = Ey_{\max} = 2.21Vot. \quad (3.24)$$


Superfluid density:

$$\Psi_0^2 = \alpha T_c / b' = \frac{m^*c^2}{4\pi e^* \lambda^2} = 7.2 * 10^{20} cm^{-3} \quad (3.25)$$

The supercurrent density:

$$J_{GL} = \frac{\hbar e^*}{m^* \xi^2} |\Psi_0|^2 = 1.7 * 10^{25} \frac{G^{1/2}}{Cm^{3/2}Sec^2} = 5.7 * 10^{15} \frac{A}{Cm^3} \quad (3.26)$$

3.3.2 Superfluid density at flux flow

In contrast to the static case, under the influence of the Lorentz force the vortices move. At low electric fields, the vortex structure approximately remains hexagonal for an isotropic material (assumed in the present study) in directions perpendicular to magnetic field. See Fig. 3.1(a) compared to perfect hexagonal lattice in statics at the same field $b = 0.4$. The moving lattice is not exactly hexagonal since electric field breaks explicitly the hexagonal symmetry,

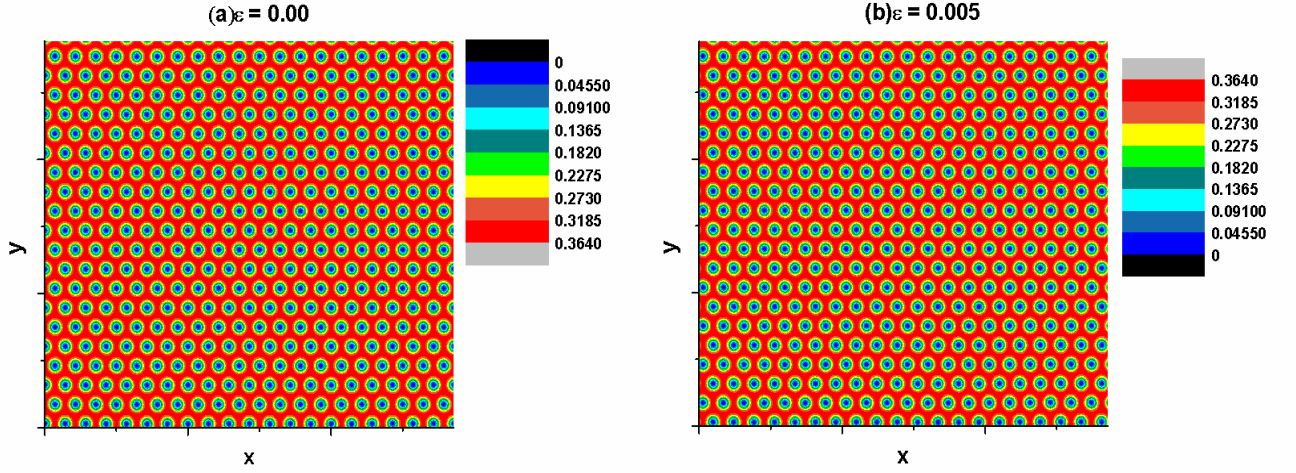


Figure 3-1: *Superfluid density with small electric field.* The picture(a) show the vortex lattice without electric field. As show in previous chapter, the vortex lattice has hexagonal symmetry. The picture(b) show the vortex lattice with small electric field. The electric field apply in y direction, and the vortices move in x direction. The moving vortex lattice is not exactly hexagonal.

see theoretical symmetry considerations in[7]. In the large electric fields, the vortex matter flows in my simulation like a liquid(In fact, the theoretical results for moving lattice still has hexagonal). For example, when I consider the vortex flow for $a_h = 0.45$ and electric field ϵ applied in the y direction, the vortex structures in different electric field show in Fig.3-1.

3.3.3 Definition of nonlinear conductivity and comparison of simulation with the analytic results

Using expansion in small parameter

$$a_h(v) = \frac{1}{2} (1 - t - b - v^2) = \frac{1}{2} \left(1 - t - b - \frac{\epsilon^2}{b^2} \right). \quad (3.27)$$

D. Li, B. Rosenstein and M. Malkin [15] calculated the nonlinear conductivity for clean type-II superconductors. In the flux flow regime, in addition to the normal state conductivity, there is a large contribution from the Cooper pairs represented by order parameter field. The nonlinear

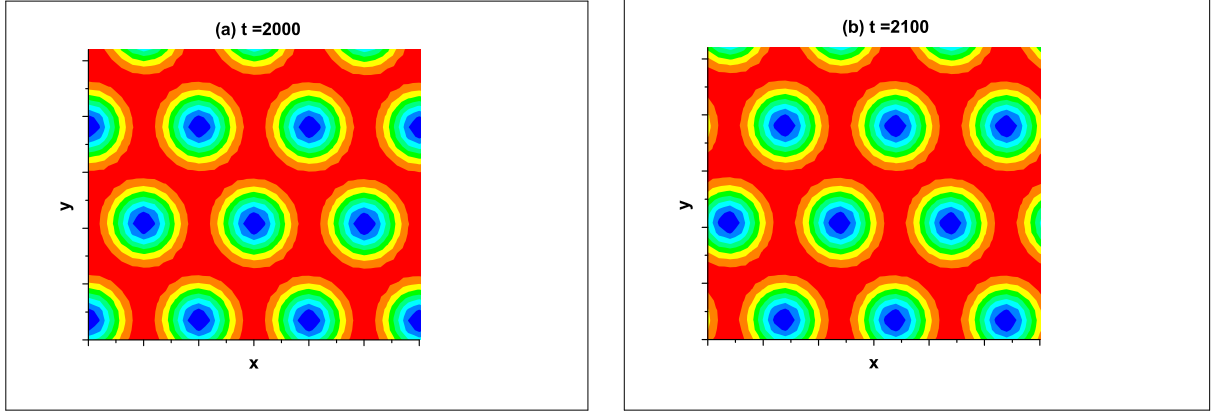


Figure 3-2: *Moving lattices with pinning.* Two snapshots at times $t=2000$ (a) and $t=2100$ (b). The vortices move in the x direction

conductivity will be defined as follows

$$\sigma_s = \frac{J_s}{E} = -\frac{i\hbar e^*}{2mE} \Psi^* \left(\nabla + \frac{ie^*}{\hbar c} \mathbf{A} \right) \Psi + cc. \quad (3.28)$$

Using the unit $\sigma_0 = \frac{4\pi\kappa^2}{c^2\gamma}$, the dimensionless nonlinear conductivity in the LLL approximation is proportional to the superfluid density,

$$\sigma_{LLL} = \frac{i}{2v} \langle \psi_{LLL}^* \partial_y \psi_{LLL} - \psi_{LLL} \partial_y \psi_{LLL}^* \rangle = \langle |\psi_{LLL}|^2 \rangle = \frac{a_h(v)}{\beta_A(v)} e^{v^2}. \quad (3.29)$$

Numerical simulation allows to check the analytic theory and extend it beyond perturbation theory applicability range.

I simulated the case $b = 0.9$, $t = 0$, for which the parameter $a_h(v) = 0.05$ is small, the order parameters are within the LLL approximation applicability range. For velocity is low (corresponding to low electric field), so that the Abrikosov beta does not change from its static value, $\beta_A(v) \simeq 1.16$. The comparison of the analytic theory and the simulation is shown in Fig.3-3. For $\beta_A(v) \neq 1.16$ at large electric field ϵ , the value for the theoretical line have to be modified. As expected, the difference between the theory and the simulation becomes smaller when $a_h(v)$ become smaller. That is, when number of Cooper pairs in becomes smaller, most of them stay in LLL.

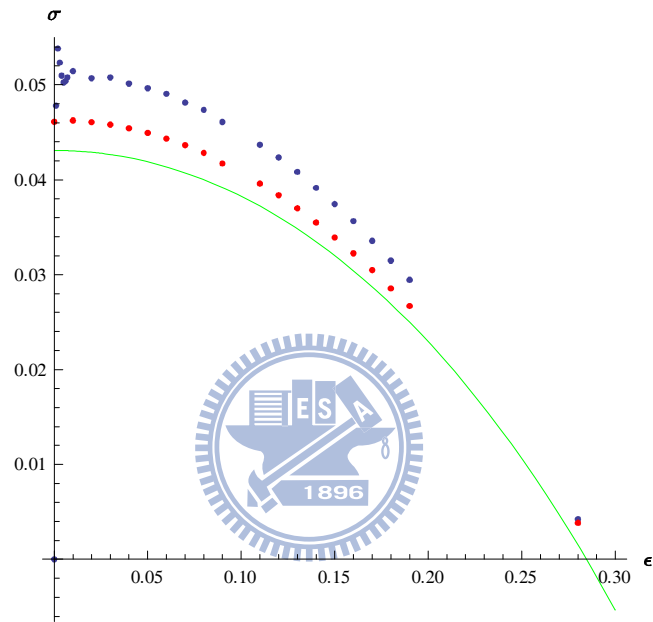


Figure 3-3: Comparison of simulated flux flow nonlinear conductivity with the analytic results. The blue points are simulation values for j/ϵ . The red points are simulation value for $\langle \psi^2 \rangle = \sigma_{LLL}$ which provides the first approximation and the green line is the full analytic expression Eq.(3.29).

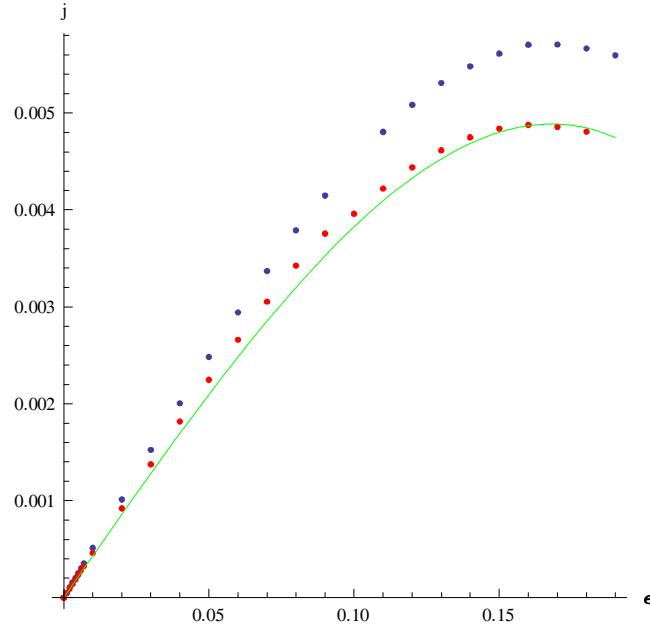


Figure 3-4: Comparison of simulated nonlinear $j - \epsilon$ curve with analytic result. The green line is theory value Eq.(3.29). The red points are simulation values for $\sigma_{LLL} * \epsilon$. The blue points are simulation for supercurrent density values.

Next, the $j - \epsilon$ characteristic is shown in Fig.3.4. The blue points are simulation result for supercurrent density, and the red points are simulation result for superfluid density multiplied by electric field, $\langle \psi^2 \rangle * \epsilon$. Note that $\langle \psi^2 \rangle$ is the LLL conductivity according to Eq.(3.29). The green line fit well with red points when a_h become small.

The theory is inapplicable when $a_h(v)$ is large, so I consider two cases with large $a_h(v)$. In the first the magnetic field b is fixed at $b = 0.4$, while temperature t' has two values 0.0 and 0.3 (just change of a_h , without thermal noise on the mesoscopic level). Electric field ϵ ranges from 0 to 0.2. The parameters $a_h(0)$ for this case are therefore, 0.3 and 0.15 respectively. See Fig.3-5. The red triangles are values for $a_h = 0.3$, while the blue squares are values for $a_h = 0.15$. The supercurrent current density at higher temperature is smaller since the temperature breaks Cooper pairs.

In the case II, the magnetic field b has two values 0.4 and 0.7, while the temperature t' is fix, $t' = 0.0$. Electric field from 0 to 0.2. The parameters $a_h(0)$ for case II are, therefore, 0.3 and 0.15 respectively. See Fig3-6. The supercurrent density in large magnetic field($b = 0.7$) is

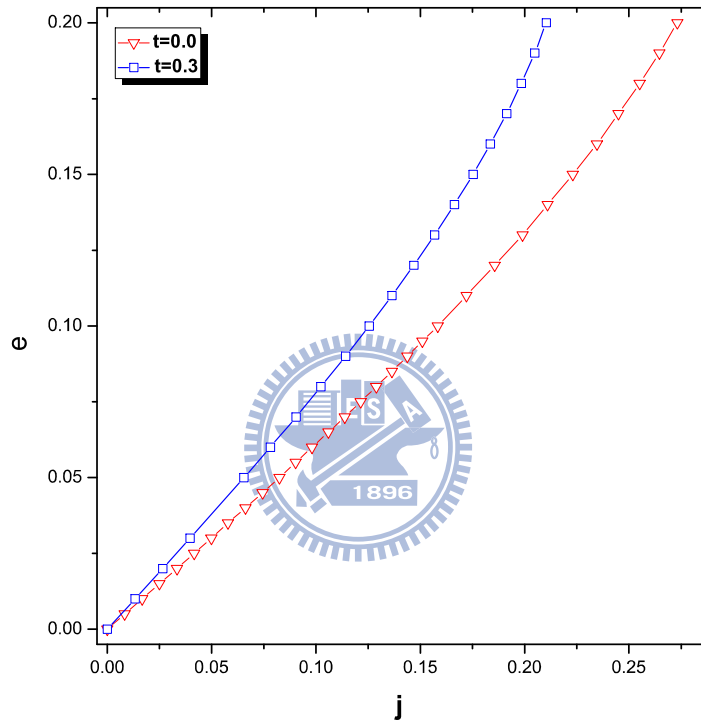


Figure 3-5: J - E curve for different a_h (fix b). The red triangles are values for $a_h(0) = 0.3$. The blue squares are values for $a_h(0) = 0.15$.

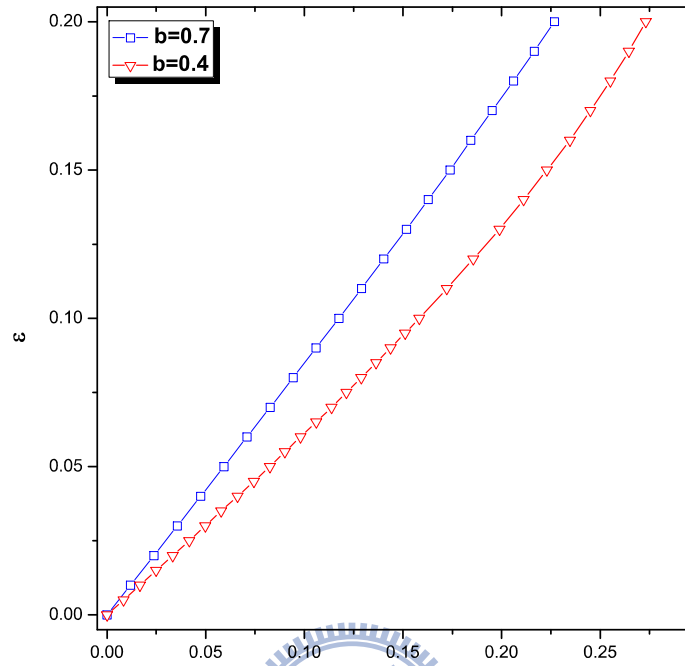


Figure 3-6: J - E curve for different a_h (fix t). The red triangles are values for $a_h(0) = 0.3$. The blue squares are values for $a_h(0) = 0.15$.

smaller the small magnetic field ($b = 0.3$) under the same electric field, for Cooper pairs density are less in large magnetic. In addition, the $j - \epsilon$ curve in $b = 0.7$ is more linear than in $b = 0.3$, the reason is that when vortex move faster, the Cooper pairs are more difficult to transport.

Chapter 4

Vortex statics and dynamics in superconductor with periodic pinning.

4.1 Time dependent Ginzburg-Landau theory with periodic pinning



The difference between the clean superconductor's GL free energy and the energy in the presence of the artificial pinning centers located \mathbf{r}_a is the pinning potential:

$$V(\mathbf{r}) = T_c \sum_a U(\mathbf{r} - \mathbf{r}_a). \quad (4.1)$$

The TDGL equation should be modified as follows

$$\frac{\gamma}{2} \frac{\hbar^2}{2m^*} \frac{\partial}{\partial t} \Psi = \frac{\hbar}{2m^*} \left(\nabla - \frac{ie}{\hbar c} \mathbf{A} \right)^2 \Psi + \alpha T_c (1 - t' + U(\mathbf{r} - \mathbf{r}_a)) \Psi - b' |\Psi|^2 \Psi. \quad (4.2)$$

Using the same units as in the clean case, the dimensionless TDGL equation becomes

$$\frac{\partial}{\partial t} \psi = \frac{1}{2} (\nabla - i\mathbf{a})^2 \psi + \frac{1}{2} (1 - t' + u(\bar{\mathbf{r}} - \bar{\mathbf{r}}_a)) \psi - (\psi^* \psi) \psi, \quad (4.3)$$

where $u(\bar{\mathbf{r}} - \bar{\mathbf{r}}_a)$ is the dimensionless pinning potential. The dimensionless current density as defined before $j = j_n + j_s$, where

$$\begin{aligned} j_n &= \sigma_{GL}\epsilon \\ j_s &= \frac{i}{2}(\psi^*\nabla\psi - \psi\nabla\psi^*) + |\psi|^2 \mathbf{a}. \end{aligned} \tag{4.4}$$

As discussed in previous, the dissipation mainly comes from the vortex flow. The electric resistance comes also from normal electrons, when the electric field is "allowed" to enter the sample due to the flux flow. Pinning slows and eventually stops vortices from moving. This is the reason why there exists the critical current.

4.2 Pinning distributions

Two kinds of pinning array are discussed in this thesis. The first one assumes that small parts of the sample are normal or even insulating. An example is the columnar defect or simply a hole. Obviously the order parameter inside such a center (neglecting the proximity effects) is always zero. The weaker δT_c pinning is just a local modification of the critical temperature at the center's site. It influences the condensation potential, Eq.(4.6). In other words, the vortices will not be always confined to the pinning centers. The simulation results are shown in following subsections.

The shape of pinning sites I simulated are rectangles. The pinning distribution is hexagonal, as shown in Fig.4-1. I assume that vortices outnumber the pinning sites, namely, the magnetic field is above the so called matching field. Therefore the filling factor parameter defined as,

$$f = \frac{\text{pinning sites' number}}{\text{vortices' number}}, \tag{4.5}$$

. For example the $f = 1/2$ case is shown in Fig.4-1

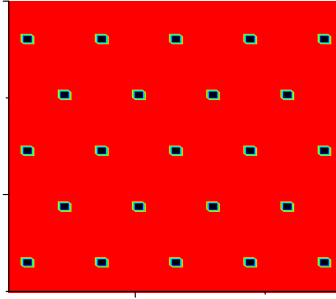


Figure 4-1: *Pinning distribution*. The black rectangles are pinning sites. The distribution of their centers is hexagonal, commensurate with the Abrikosov lattice.

4.3 Strong pinning array

The magnetic field $b = 0.4$ and the temperature $t = 0$ in the following simulation.

4.3.1 Superfluid density

The vortex distribution is influenced by pinning. In this simulation all the pinning distributions are hexagonal, however the size of the pinning sites varies (pinning size 4, 9, 16). The pinning factor $f = 0.5$. The results are shown in Fig.4-2~Fig.4-4. In Fig.4-2 for the size of 4, the vortex structure still has hexagonal symmetry, while for larger sized in Fig.4-3 and Fig.4-4, the vortex structure does not remain hexagonal.

4.3.2 Dynamics in the presence of pinning.

a. Interstitial vortices

The vortices in the superconductors with artificial pinning array can be separated into two different sets: the pinned vortices which are trapped on the pinning centers, and the interstitial vortices which can be considered as "free vortices". If the number of vortices is smaller than the number of pinning sites, all of them are likely to be pinned. If magnetic field is equal to the matching field, there are no interstitial vortices, however when vortices outnumber the

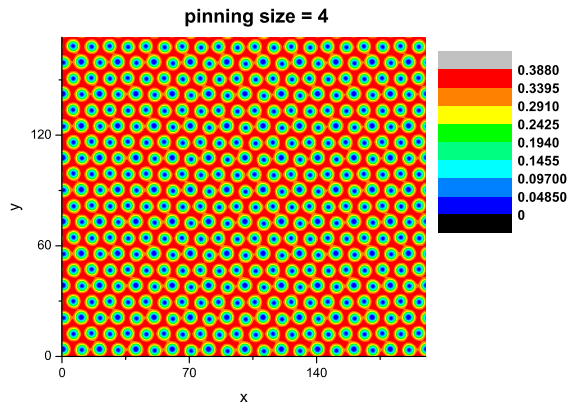


Figure 4-2: *Vortex structure with periodic pinning (pinning size = 4)*. The vortex lattice still has hexagonal symmetry, while the vortex core in the pinning centers are larger than that of the interstitial vortices.

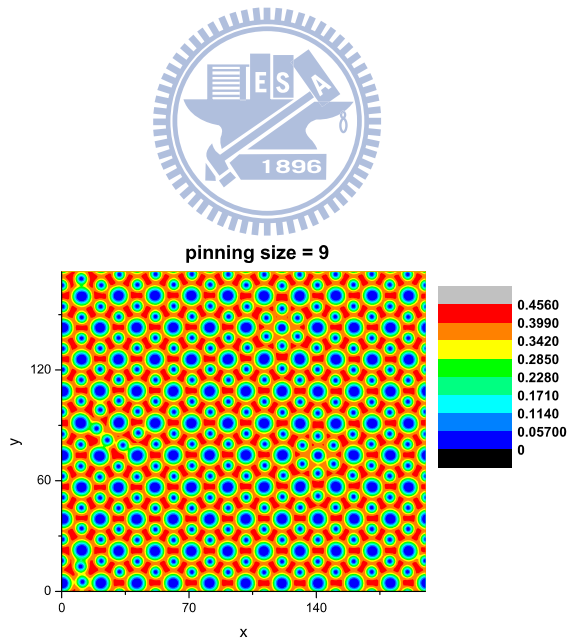


Figure 4-3: *Vortex structure with periodic pinning (pinning size = 9)*. The vortex structure is different compared to the clean system. Pinning leads to expansion of the vortex cores.

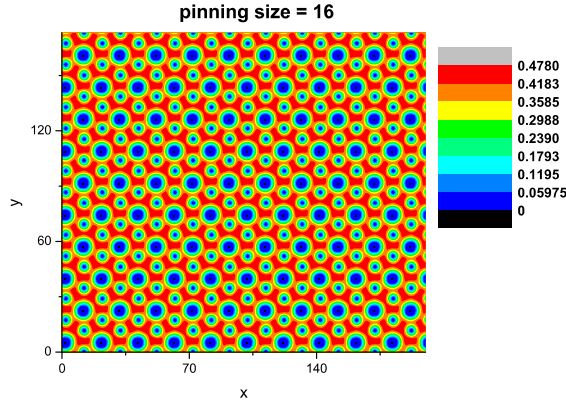


Figure 4-4: *Vortex Structure with periodic pinning*(pinning size = 16). Similar to Fig.4-3, the pinning vortices lead the vortex distortion increasing the unit cell

sites, some of them will be "liberated" due to repulsion from the vortices already pinned. On Fig.4-5 the dynamics of the interstitial vortices is shown. The electric field is applied in the y direction, thus the vortices move along the x direction. The parameters for the simulation are: the electric field $\epsilon = 0.0001$. Pinning centers size is 4. Two snapshots at times $t = 2000$ (a) and $t = 2100$ (b) for the case when for each rectangular pinning center there are two vortices. Two different kinds of vortices are seen: the interstitial vortices have smaller cores and move, and the pinned vortices which have larger cores (like in the static case) and don't move.

For the pinning force is larger than the driving force, the pinned vortices are not moving, while the interstitial are pushed by driving force. The flux flow therefore is due to interstitial vortices.

b. I-V curves

In this subsection the dependence of the flux flow current on the electric field is presented. One should be warned that the simulation is reliable only when the supercurrent is smaller than the normal current. Otherwise the electric field in the superconductors is not uniform and a much more complicated system of equations including the Maxwell equations for the electric field should be solved. Thus the simulation results for currents approaching the critical current

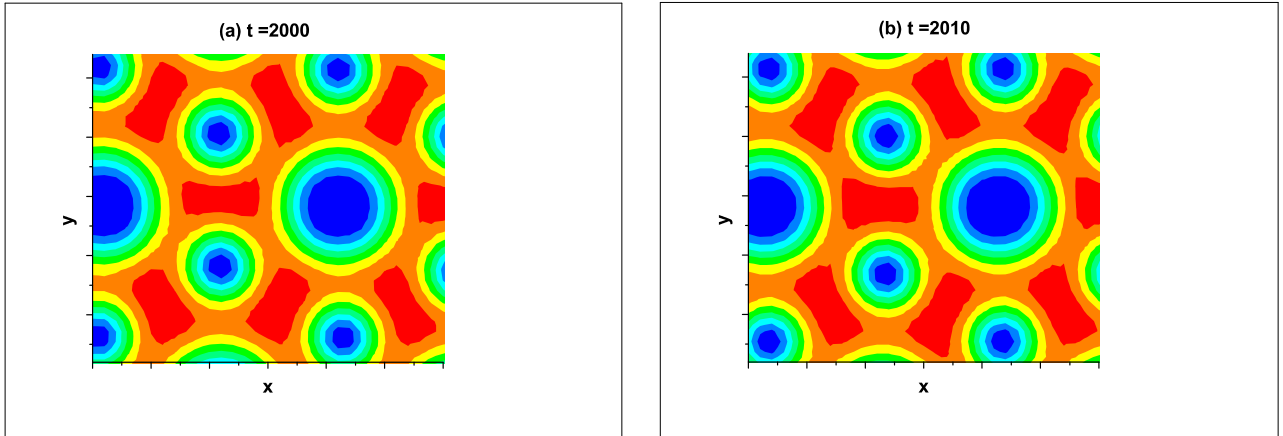


Figure 4-5: *Moving lattices with pinning.* Two snapshots at times $t=2000$ (a) and $t=2100$ (b) for the case when for each rectangular pinning center there are two vortices. Two different kinds of vortices are seen: the interstitial vortices have smaller cores and move, and the pinned vortices which have larger cores and don't move.

are not correct.

In Fig. 4-6, the $J - E$ curves for the clean superconductors and the superconductors with pinning array are compared. The parameters in the simulation are: the electric field ϵ from 0 to 0.2, pinning factor $f = 0$ (clean) and 0.5. The size of pinning centers is 9. When the electric field is large the behavior of $J - E$ curve for the clean superconductors and superconductors with pinning array are similar. However when electric field is small but larger than pinning force, the current for superconductors with pinning array is larger than the clean superconductors. The reason is that the pinning array reduces the velocity of moving vortices. If the driving force is smaller than the pinning, the resistance is zero inside the superconductors.

4.4 Weaker pinning array

The magnetic field $b = 0.4$ and the temperature $t = 0$ in the following simulation.

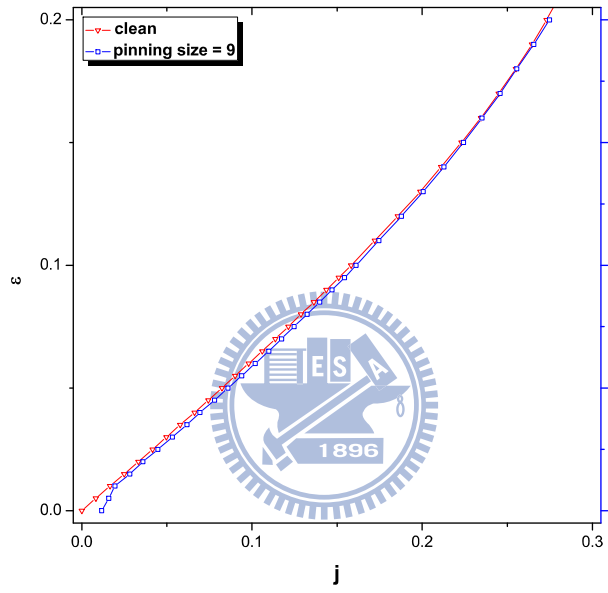


Figure 4-6: Comparison $J-E$ curve for clean superconductors and superconductors with pinning array. The red triangle represent clear system. The blue rectangle represent system with pinning in size of 9.

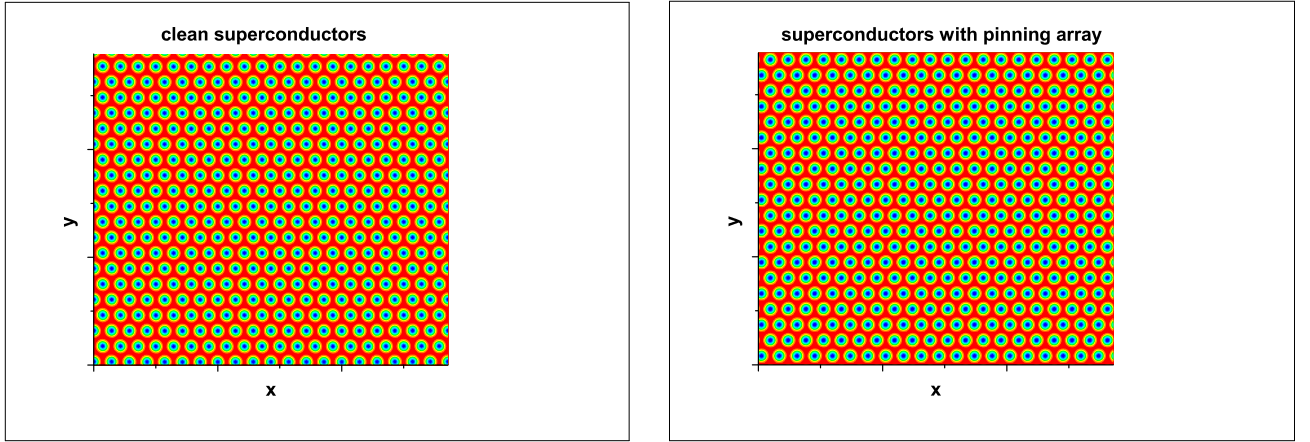


Figure 4-7: *Comparison of vortex lattices for clean superconductors and superconductors with pinning array.* The picture in the left hand side show the vortex lattice in clean superconductors, and the picture in the right hand side show the vortex lattice in superconductors with pinning array. The different between two pictures is that the positions of vortices are shifted by the pinning array.

4.4.1 Superfluid density

The comparison of vortex lattice for the clean superconductors and superconductors with pinning array is shown in Fig.4-7. The pinning factor $f = 0$ (clean) and 1, and the pinning size is 9. As Fig.4-7 shown, the vortices are trapped on the pinning centers. The pinned vortices in strong pinning array and in weaker pinning array are different. For the strong pinning array the size of vortex cores dependent on the pinning size (see Fig.4-3), while for the weaker pinning array the size of vortex cores is almost the same as vortex in clean superconductors.

4.4.2 I-V curves

The condensation potential is influenced by the pinning array, it can be seem as the critical temperature is changed. The average condensation potential is modified as following

$$\frac{1}{N} \sum_{n=1}^N - (1 - t - u(r_n - r_a)) = \frac{1}{N} \sum_{n=1}^N - (1 - t'), \quad (4.6)$$

where r_a represent the pinning positions, t is the original critical temperature and t' is the new critical temperature. Note that $t' > t$, which means the critical temperature T_c become smaller. However, this work compared systems with the same critical temperature, a constant ζ is added into the condensation potential, so that

$$\frac{1}{N} \sum_{n=1}^N - (1 - t - u(r_n - r_a) + \zeta) = \frac{1}{N} \sum_{n=1}^N - (1 - t), \quad (4.7)$$

where

$$\zeta = \frac{\sum_{n=1}^N u(r_n - r_a)}{N}. \quad (4.8)$$

The comparison of $J - E$ cures for different strength of pinning potentials as shown in Fig.4-8. The parameters for the simulation are: the electric field form 0 to 0.4. The pinning factor $f = 1$, and size of pinning center is 1. The strength of pinning potential are 0 (clean system), 1 and 10. The values of critical current are dependent on the strength of pinning potential. When pinning potential is large, the vortices are more difficult to escape from the pinning centers. The resistance is zero when vortices are trapped. As shown in Fig4-8, the superconductors with pinning array can bear stronger electric field. The reason is the velocity of moving vortices is reduced by the pinning force, in other words, the energy dissipation is reduced. All in all, the pinning effect increase both the critical current and critical electric field (critical velocity of moving lattice), while the critical temperature is decrease.

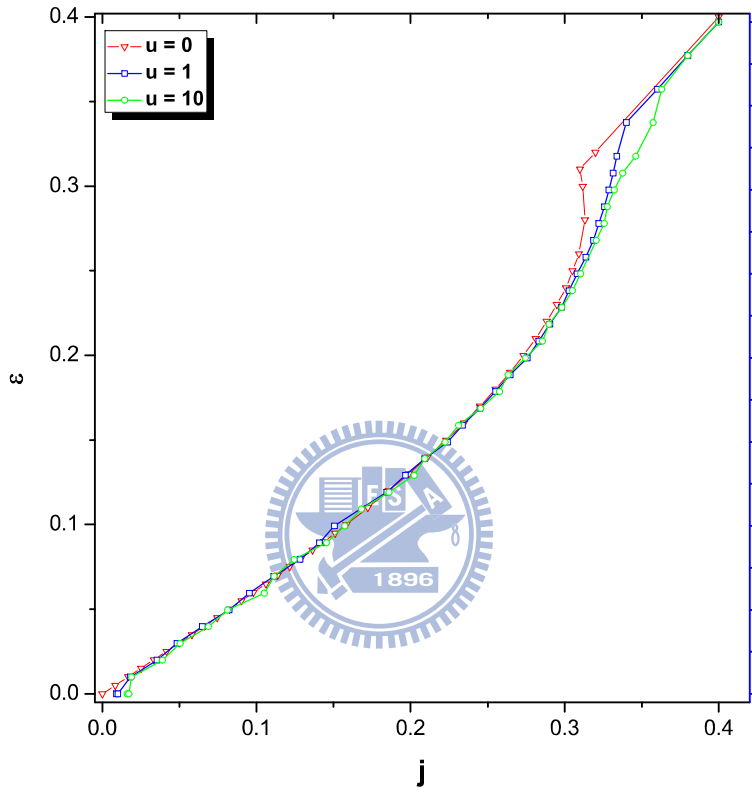


Figure 4-8: Comparison of $J - E$ curve for different strength of pinning potential ($u = 0, u = 0.5, u = 1$). The red triangles are values for clean superconductor, the blue circle are values for superconductors with weaker pinning array ($u = 1$), the purple diamond are values for superconductors with stronger pinning array ($u = 10$). The pinning effects are obvious when electric field is small, and when electric field near critical electric field.

Chapter 5

Conclusion

The statics and dynamics of vortex lattices in highly anisotropic layered type II superconductors has been studied by using the 2D time-dependent Ginzburg-Landau equation. The $U - \psi$ algorithm was used to simulate the TDGL equation numerically. Both the order parameters describing the vortex lattice and the non-linear $J - E$ characteristics were calculated. Two different cases were investigated in this thesis, one is the clean superconductors and another one is superconductors with artificial pinning array commensurate with Abrikosov lattice.

In clean superconductors, the static superfluid density (square of the order parameter $|\psi|^2$) decreases as the magnetic field increases approaching the upper critical field $H_{c2}(T)$ and vanishes when magnetic field is larger than $H_{c2}(T)$. The static configuration of vortex lattice has hexagonal symmetry. When the electric field enters the superconductors, the vortices would move due to the Lorentz force and the vortex configuration is deformed. Furthermore, the superfluid density also decreases with electric field increase. The relation between superfluid density, magnetic field and electric field are well represented by the bifurcation expansion formula $|\psi|^2 = a_h/\beta_A$, where the parameter $a_h = (1 - t - b - \frac{\xi^2}{b^2})/2$ (the superfluid density becoming zero when $a_h \leq 0$). Deviations from this formula at large currents (electric fields) were found. In small electric field region the $J - E$ characteristic is linear, while in large electric field the $J - E$ characteristic is non-linear. The simulation result for $J - E$ characteristic fit in with analytical result in small a_h . I also compared $J - E$ characteristics with different a_h including different temperature t and different magnetic field b .

In superconductors with artificial pinning array, the vortices are trapped by the pinning

centers. Two different strength of pinning arrays are considered in this work. I compared vortex configuration in statics and dynamics for different pinning sizes (from small to large), numbers and kinds (from a very strong pinning by a normal islands to weak δT_c pinning). The order parameter and supercurrent configuration, which is in clean material dominated by the repulsive inter - vortex forces is deformed by the pinned vortices. The $J - E$ characteristics are also strongly influenced by the pinning array. When the electric field is smaller than the pinning force, the vortices are standing on the pinning centers and reduce the energy dissipation(Joule heat). When the electric field is larger than the pinning force, the velocity of moving vortex is reduced by the pinning array. Therefore the superconductors with pinning array can bear stronger electric field. All in all, the pinning effect increase both the critical current and critical electric field (critical velocity of moving lattice), while the critical temperature is decrease.

The model in this thesis only consider the uniform electric field, therefore this model only can applied when normal current is larger than supercurrent. The full electrodynamics have to be considered when normal current smaller than supercurrent. In addition, the model does not contain the influence of thermal fluctuation which are especially important for high T_c superconductors. When temperature approach T_c , the thermal fluctuation would dominate the physical quantities such as vortex structure (structure factor), heat capacity and conductivity. In the future, the full electrodynamics and thermal noise would add into the model.

Bibliography

- [1] S. B. Field et al., Phys. Rev. Lett. **88**, 067003 (2002).
- [2] V.R. Misko, S. Savel'ev and F. Nori, Phys. Rev. Lett. **95**, 094512 (2005)
- [3] J. E. Villegas, M. I. Montero, C.-P. Li, and I. K. Schuller, Phys. Rev. Lett. **97**, 027002 (2006).
- [4] J.-Y. Lin, M. Gurvitch, S. K. Tolpygo, A. Bourdillon, S. Y. Hou and J. M. Phillips, Phys.Rev. B **54**, R12717 (1996); S. Goldberg, Y. Segev, Y. Myasoedov, I. Gutman, N. Avraham, M. Rappaport, E. Zeldov, T. Tamegai, C. W. Hicks, and K. A. Moler, Phys. Rev. B **79**, 064523 (2009).
- [5] C. Reichhardt, C. J. Olson and F. Nori, Phys. Rev. Lett. **78**, 2648 (1997); Phys. Rev. B **58**, 6534 (1998); C. Reichhardt, G. T. Zimanyi and N. Gronbech-Jensen, Phys. Rev. B **64**, 014501 (2001); C. Reichhardt and C. J. Olson Reichhardt, Phys. Rev. B **79**, 134501 (2009).
- [6] C. C. de Souza Silva, J. A. Aguiar and V. V. Moshchalkov, Phys. Rev. B **68**, 134512 (2003); Q. H. Chen, C. Carballeira, T. Nishio, B. Y. Zhu, and V. V. Moshchalkov, Phys. Rev. B **78**, 172507 (2008).
- [7] B. Rosenstein and D.P. Li, Rev. Mod. Phys. in press (2009).
- [8] D.Li, and B. Rosenstein, Phys. Rev. B **60**, 10460 (1999).
- [9] H. J. Jensen , A. Brass and A. J. Berlinsky, Phys. Rev. Lett. **60**, 1676 (1988); H. J. Jensen, A. Brass, Y. Brechet and A. J. Berlinsky, Phys. Rev. B **38**, 9235 (1988); A.C. Shi and A.

- J. Berlinsky, Phys. Rev. Lett. **67**, 1926 (1991); B. Y. Zhu, J. Dong, and D. Y. Xing, Phys. Rev. B **57**, 5063 (1998); H. Fangohr, S. J. Cox and P. A. J. de Groot, Phys. Rev. B **64**, 064505 (2001); A.B. Kolton, D. Dominguez and N. Gronbech-Jensen, Phys. Rev. Lett. **86** 4112 (2001).
- [10] J. F. Annett, Superconductivity superfluids and condensates Oxford(2003)
- [11] Y.Kato, and N. Nagaosa, Phys. Rev. B **47**, 2932(1993); **48**, 7383(1993)
- [12] J.Hu, and A. H. MacDonald, Phys. Rev. Lett. **71**, 432(1993);Phys. Rev. B **56**, 278(19978)
- [13] M. S. Li, and T. Natterman, Phys. Rev. B **67**, 194520(2003)
- [14] D.LI, B, Rosenstein and V. Vinokour, Jourenal of superconductivity and Novel Magnetism **19**, 369(2006)
- [15] D.LI, B, Rosenstein, and M. Malkin, Phys. Rev. B **70**, 214529(2004)
- [16] B. Rosenstein and V. Zhuravlev, Phys. Rev. B **76**, 014507 (2007)
- [17] H. J. Rithe, Lattice Gauge Theories An Introduction(World Science 2005); L.E. Reichl, A Moden Course in Statistical Physics(John Wiley 1998)
- [18] J. Crank, and P. Nicolson Comp. Math. **6**(1996)207-226;J. B. Chen, Journal of the Physical Society of Japan **71**, 2348
- [19] D. Y. Vodoiazov, and F. M. Peeters, Phys. Rev. B **76**, 014521(2007)
- [20] J. Deang, Q. Du, and M. D. Gunzburger, Phys. Rev. B **64**, 052506(2001)
- [21] W. D. Gropp, H.G. Kapper, G.K. Leaf, D. M. Levine, M. Palumbo and V. M Vinokur, Journal of computational physics**123**, 254-266(1996)
- [22] M. Machida, and H. Kaburaki, Phys. Rev. Lett **71**, 3206
- [23] A. Mourachkine, Hight-Temperature Superconductivity in Cuprates, 2002 Kluwer Academic Publishers
- [24] N. W. Ashcroft, and N. D. Mermin, Solid State Physics, Tomoson Learning(1976)

- [25] Hoffman Lab, Dept. of Physics Harvard University
- [26] J. Gutierrez, A. V. Silhanek, J. Van de Vondel, W. Gillijns, and V. V. Moshchalkov, Phys. Rev. B **80**, 140514(2009)
- [27] R. Kato, Y. Enomoto, and S. Maekawa, Phys. Rev. B **47**, 8016 (1993)
- [28] S. Mukerjee and D. A. Huse, Phys. Rev. B **70**, 014506 (2004)
- [29] J. Blatter, M. V. Feigelman, V. B. Geshkenbein, A. I. Larkin, and V. M. Vinokur, Rev. Mod. Phys. **66**, 1125 (1994).
- [30] Kopnin, "Vortices in type-II superconductors: Structure and Dynamics", Chernogolovka, (1995).
- [31] B. L. T. Plourde et al, PRB **66**, 054529(2002)
- [32] M. Tinkham, Introduction to Superconductivity(McGraw-Hill, New York 1996)
- [33] J. B. Kogut, Rev. Mod. Phys. 51, 659(1979); J. B. Kogut, Rev. Mod. Phys 55, 775(1983); H. J. Rithe, Lattice Gauge Theories An Introduction(World Science 2005)
- [34] T. Zak, Phys. Rev 134, 6A(1963); J. Chee, Physics Letters A 275(2000)473; A. Wal, Journal of Physics:Conference Series 30(2006)286
- [35] Q. Du, M. D. Gunzburger, and J. S. Peterson, Phys. Rev. B **51**, 16194 (1995)
- [36] R. L. Burden and J. D. Faires, Numerical Analysis(Thomson 2005)

Appendix A

Dimensionless formulas

Start from physical unit Gibb's free energy without pinning potential

$$\begin{aligned}
 F &= \int d^2\mathbf{r} \frac{\hbar^2}{2m^*} \left| \left(\nabla - \frac{ie^*}{\hbar c} \mathbf{A} \right) \Psi \right|^2 - \alpha T_c (1-t) |\Psi|^2 + \frac{b'}{2} |\Psi|^4 \\
 &= \int d^2r F_n
 \end{aligned} \tag{A.1}$$

with $\alpha T_c = \frac{\hbar^2}{2m^*\xi^2}$, $b' = \frac{2\pi\hbar^2\lambda^2 e^{*2}}{\xi^2 c^2 m^{*2}}$, where F_n is energy density. Let unit of length is ξ , unit of gauge is $H\xi$, unit of order parameter is $\sqrt{2}\Psi_0 = \sqrt{2(\alpha T_c)/b'}$, the equation above can be write as following

$$\frac{F}{b' |\Psi_0|^4} = \frac{\hbar^2}{2m^* b' |\Psi_0|^4} \left| \left(\frac{1}{\xi} \nabla' - \frac{ie^*}{\hbar c} (H_c \xi a) \right) \Psi \right|^2 - \frac{\alpha T_c}{b' |\Psi_0|^4} (1-t) |\Psi|^2 + \frac{1}{2} |\psi|^4, \tag{A.2}$$

where $\frac{1}{b' |\Psi_0|^4} = \frac{\hbar^2 c^2}{8\pi \xi^2 \lambda^2 e^{*2}} = \frac{(H_c \xi^2)^2}{8\pi \xi^2 \lambda^2} = \frac{H_c^2}{8\pi \kappa^2}$, and $\frac{e^* H_c \xi^2}{\hbar c} = \frac{2\pi}{\Phi_0} H_c \xi^2 = 1$. Let dimensionless energy $f = \frac{8\pi \kappa^2}{H_c^2} F$, therefore the dimensionless Gibb's free energy can rewrite as following

$$f = \int d^2\mathbf{r} \frac{1}{2} |(\nabla' - ia) \psi|^2 - \frac{(1-t)}{2} |\psi|^2 + \frac{1}{2} |\psi|^4. \tag{A.3}$$

Next, I chose symmetric gauge, $\mathbf{A} = \left(\frac{-1}{2} B y, \frac{1}{2} B x - c E t \right)$, while the dimensionless gauge as

following

$$\begin{aligned}\mathbf{a} &= \frac{\mathbf{A}}{H_c \xi} = \left(\frac{-1}{2} \frac{By}{H_c \xi}, \frac{1}{2} \frac{Bx}{H_c \xi} - \frac{cEt}{H_c \xi} \right) \\ &= \left(\frac{-1}{2} b\bar{y}, \frac{1}{2} b\bar{x} - \epsilon\bar{t} \right),\end{aligned}\tag{A.4}$$

with $\epsilon = E/E_{GL}$, $\bar{t} = t/t_{GL}$, where unit of electric field $E_{GL} = \frac{\xi}{ct_{GL}} H_c c_2 = \frac{2}{c\gamma\xi} H_c c_2$.

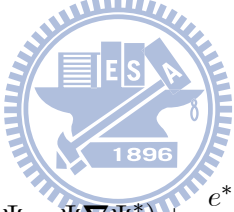
Third, the TDGL equation

$$\frac{\gamma}{2} \frac{\hbar^2}{2m^*} \frac{\partial \psi}{\partial t} = - \frac{\delta f}{\delta \psi^*};\tag{A.5}$$

$$\begin{aligned}\frac{\partial \psi}{\partial \bar{t}} &= - \frac{\delta f}{\delta \psi^*} \\ &= \frac{1}{2} (\nabla' - i\mathbf{a})^2 \psi - \frac{(1-t)}{2} \psi + |\psi|^2 \psi,\end{aligned}\tag{A.6}$$

with the unit of time $t_{GL} = \frac{\gamma \hbar^2}{4m^*}$.

Finally, supercurrent density,



$$\begin{aligned}\mathbf{J}_s &= \frac{i\hbar e^*}{2m^*} (\Psi^* \nabla \Psi - \Psi \nabla \Psi^*) + \frac{e^*}{m^* c} \mathbf{A} |\Psi|^2 = \frac{e^* \hbar}{m^* \xi} |\Psi_0|^2 j_s \\ &= \frac{cH_c c_2}{2\pi \xi \kappa^2} j_s,\end{aligned}\tag{A.7}$$

where $\frac{cH_c c_2}{2\pi \xi \kappa^2} = \frac{c \frac{\hbar c}{\xi^2 e^*}}{2\pi \xi \kappa^2} = \frac{\hbar c^2}{e^* 2\pi \xi \lambda^2} = \frac{\hbar c^2}{e^* 2\pi \xi} \frac{e^{*2} 4\pi |\Psi_0|^2}{m^* c^2} = \frac{2\hbar e^*}{m^* \xi}$, and $\frac{e^* H_c \xi^2}{ch} = \frac{2\pi}{\Phi_0} H_c \xi^2 = 1$, therefore the dimensionless supercurrent density

$$j = \frac{i}{2} (\psi^* \nabla' \psi - \psi \nabla' \psi^*) + |\psi|^2 \mathbf{a}.\tag{A.8}$$

Appendix B

Link variables

The link variable vector U define as following

$$U = \exp(-i\theta_{n_1, n_2}^\gamma), \quad (\text{B.1})$$

where phase $\theta_{n_1, n_2}^\gamma = \int_n^{n+\mu^\gamma/s} \mathbf{a} \cdot d\mathbf{r}$ is the Aharonov-Baohm(A-B) phase, with \mathbf{a} is the dimensionless vector potential, n is the link's origin, while it ends at $n + (a_\Delta/s) \mu^\gamma$.he line integral is taken along the straight line. In order to simplify the calculation of the line integration, we define a parameter $0 < \alpha < 1$:

$$\frac{d}{d\alpha} \mathbf{r}^\gamma(\alpha) = \frac{a_\Delta}{s} \boldsymbol{\mu}_\gamma,$$

where $\gamma = 1, 2, 3$ and $\boldsymbol{\mu}_\gamma$ is the unit vector.

The general formula for θ_{n_1, n_2}^γ is

$$\begin{aligned} \theta_{n_1, n_2}^\gamma &= \int_0^1 d\alpha \left\{ \left[\frac{d}{d\alpha} x^\gamma(\alpha) \right] a_x(\mathbf{r}^\gamma(\alpha)) + \left[\frac{d}{d\alpha} y^\gamma(\alpha) \right] a_y(\mathbf{r}^\gamma(\alpha)) \right\} \\ &= \frac{a_\Delta}{s} \int_0^1 d\alpha \{ \mu_x a_x(\mathbf{r}^\gamma(\alpha)) + \mu_y a_y(\mathbf{r}^\gamma(\alpha)) \}, \end{aligned} \quad (\text{B.2})$$

where a_x and a_y were defined in Eq.(A.4). For hexagonal grid, the unit vectors are

$$\mu_1 = (1, 0); \mu_2 = \left(\frac{1}{2}, \frac{\sqrt{3}}{2} \right); \mu_3 = \left(\frac{-1}{2}, \frac{\sqrt{3}}{2} \right),$$

The A-B phase for μ_1 direction:

$$\mathbf{r}^1(\alpha) = \frac{a_\Delta}{s} \left(n_1 + \alpha + \frac{n_2}{2}, \frac{\sqrt{3}}{2} n_2 \right) \rightarrow \quad (\text{B.3})$$

$$\begin{aligned} \theta_{n_1, n_2}^1 &= \frac{a_\Delta}{s} \int_0^1 d\alpha \frac{-1}{2} b\bar{y} \\ &= -\frac{\sqrt{3}}{2} \frac{a_\Delta^2}{s^2} b n_2 \end{aligned} \quad (\text{B.4})$$

Similarly, the A-B phase for μ_2 and μ_3 direction

$$\mathbf{r}^2(\alpha) = \frac{a_\Delta}{s} \left(n_1 + \frac{n_2 + \alpha}{2}, \frac{\sqrt{3}}{2} (n_2 + \alpha) \right) \rightarrow \quad (\text{B.5})$$

$$\begin{aligned} \theta_{n_1, n_2}^2 &= \frac{a_\Delta}{s} \int_0^1 \left[\frac{1}{2} b\bar{y} + \frac{\sqrt{3}}{2} (b\bar{x} - \epsilon\bar{t}) \right] d\alpha \\ &= \frac{\sqrt{3}}{4} \frac{a_\Delta^2}{s^2} b n_1 - \frac{\sqrt{3}}{2} \epsilon\bar{t}; \end{aligned} \quad (\text{B.6})$$

$$\mathbf{r}^3(\alpha) = a \left(n_1 - \alpha + \frac{n_2 + \alpha}{2}, \frac{\sqrt{3}}{2} (n_2 + \alpha) \right) \rightarrow \quad (\text{B.7})$$

$$\begin{aligned} \theta_{n_1, n_2}^3 &= \frac{ba}{2} \int_0^1 \left[\frac{1}{2} \frac{\sqrt{3}}{2} \bar{y} + \frac{\sqrt{3}}{2} (b\bar{x} - \epsilon\bar{t}) \right] d\alpha \\ &= \frac{\sqrt{3}}{4} \frac{a_\Delta^2}{s^2} b (n_1 + n_2) - \frac{\sqrt{3}}{2} \epsilon\bar{t}. \end{aligned} \quad (\text{B.8})$$

For rectangular grid, the unit vectors are

$$\mu_1 = (1, 0); \mu_2 = \left(0, \frac{\sqrt{3}}{2} \right). \quad (\text{B.9})$$

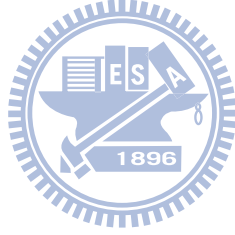
The A-B phase for μ_1 and μ_2 directions

$$\mathbf{r}^1(\alpha) = \frac{a_\Delta}{s} \left(n_1 + \alpha, \frac{\sqrt{3}}{2} n_2 \right) \rightarrow \quad (\text{B.10})$$

$$\begin{aligned} \theta_{n_1, n_2}^1 &= \frac{a_\Delta}{s} \int_0^1 d\alpha \frac{-1}{2} b\bar{y} \\ &= -\frac{\sqrt{3}}{4} \frac{a_\Delta^2}{s^2} b n_2; \end{aligned} \quad (\text{B.11})$$

$$\mathbf{r}^2(\alpha) = \frac{a_\Delta}{s} \left(n_1, \frac{\sqrt{3}}{2} (n_2 + \alpha) \right) \rightarrow \quad (\text{B.12})$$

$$\begin{aligned} \theta_{n_1, n_2}^1 &= \frac{a_\Delta}{s} \int_0^1 \frac{\sqrt{3}}{2} d\alpha \left(\frac{1}{2} b\bar{x} - \epsilon\bar{t} \right) \\ &= \frac{\sqrt{3}}{4} \frac{a_\Delta^2}{s^2} b n_2 - \frac{\sqrt{3}}{2} \epsilon\bar{t}. \end{aligned} \quad (\text{B.13})$$



Appendix C

Continuum limit

In this work, I introduced lattice gauge theory to get the discretized TDGL equation and free energy. This appendix proof that the limit of discretized formulas are the same as continuum formulas. About the free energy on hexagonal grid:

$$f = \sum_{n_1, n_2=1}^{n_{\max}} f_{\text{grad}} + f_{\text{pot}}; \quad (\text{C.1})$$

$$f_{\text{grad}} = - \left(\frac{\sqrt{3}}{2} \right) \sum_{n_1, n_2=1}^{n_{\max}} \frac{2}{3} \psi_{n_1, n_2}^* \left\{ \begin{array}{l} \left[\begin{array}{l} (U_{n_1, n_2}^1 \psi_{n_1+1, n_2} - \psi_{n_1, n_2}) + \\ (U_{n_1, n_2}^2 \psi_{n_1, n_2+1} - \psi_{n_1, n_2}) + \\ (U_{n_1, n_2}^3 \psi_{n_1-1, n_2+1} - \psi_{n_1, n_2}) \end{array} \right] \\ + cc \end{array} \right\} \quad (\text{C.2})$$

$$f_{\text{pot}} = \frac{\sqrt{3}}{2} d^2 \sum_{n_1, n_2=1}^{n_{\max}} \left[- (1 - t') |\psi_{n_1, n_2}|^2 + \frac{1}{2} |\psi_{n_1, n_2}|^4 \right],$$

with lattice distance $\frac{a\Delta}{s} = d$, where symbol U represent the link variable which defined in Eq.(B.1).

$$\begin{aligned}
f_{\text{grad}} &= -\frac{2}{\sqrt{3}} \sum_{n_1, n_2=1}^{n_{\text{max}}} \psi_{n_1, n_2}^* \left\{ \begin{array}{l} \exp(-i\theta_{n_1, n_2}^1) \psi_{n_1+1, n_2} + \\ \exp(i\theta_{n_1, n_2}^1) \psi_{n_1-1, n_2} + \\ \exp(-i\theta_{n_1, n_2}^2) \psi_{n_1, n_2+1} + \\ \exp(i\theta_{n_1, n_2}^2) \psi_{n_1, n_2-1} + \\ \exp(-i\theta_{n_1, n_2}^3) \psi_{n_1-1, n_2+1} + \\ \exp(i\theta_{n_1, n_2}^3) \psi_{n_1+1, n_2-1} \end{array} \right\} - 6\psi_{n_1, n_2} \quad (\text{C.3}) \\
&= \frac{2}{\sqrt{3}} \sum_{n_1, n_2=1}^{n_{\text{max}}} \psi_{n_1, n_2}^* \left\{ \begin{array}{l} \left(1 - i\theta_{n_1, n_2}^1 + \frac{(\theta_{n_1, n_2}^1)^2}{2}\right) \psi_{n_1+1, n_2} + \\ \left(1 + i\theta_{n_1, n_2}^1 + \frac{(\theta_{n_1, n_2}^1)^2}{2}\right) \psi_{n_1-1, n_2} + \\ \left(1 - i\theta_{n_1, n_2}^2 + \frac{(\theta_{n_1, n_2}^2)^2}{2}\right) \psi_{n_1, n_2+1} + \\ \left(1 + i\theta_{n_1, n_2}^2 + \frac{(\theta_{n_1, n_2}^2)^2}{2}\right) \psi_{n_1, n_2-1} + \\ \left(1 - i\theta_{n_1, n_2}^3 + \frac{(\theta_{n_1, n_2}^3)^2}{2}\right) \psi_{n_1-1, n_2+1} + \\ \left(1 + i\theta_{n_1, n_2}^3 + \frac{(\theta_{n_1, n_2}^3)^2}{2}\right) \psi_{n_1+1, n_2-1} \end{array} \right\} - 6\psi_{n_1, n_2}.
\end{aligned}$$

Expand the order parameters ψ_{n_1+1, n_2} , ψ_{n_1, n_2+1} , and ψ_{n_1-1, n_2+1} by using Taylor explanation. The Eq.(C.3) become as following

$$\begin{aligned}
f_{\text{grad}} &= -\frac{2}{\sqrt{3}} \sum_{n_1, n_2=1}^{n_{\text{max}}} \psi_{n_1, n_2}^* \left\{ \begin{array}{l} \left[(\theta_{n_1, n_2}^1)^2 + (\theta_{n_1, n_2}^2)^2 + (\theta_{n_1, n_2}^3)^2 \right] \psi_{n_1, n_2} + \\ -id \left[2\theta_{n_1, n_2}^1 - \theta_{n_1, n_2}^2 + \theta_{n_1, n_2}^3 \right] \frac{\partial \psi_{n_1, n_2}}{\partial x} + \\ -id\sqrt{3} \left[\theta_{n_1, n_2}^2 + \theta_{n_1, n_2}^3 \right] \frac{\partial \psi_{n_1, n_2}}{\partial y} + \\ \frac{3}{2} \frac{\partial^2 \psi_{n_1, n_2}}{\partial x^2} + \frac{3}{2} \frac{\partial^2 \psi_{n_1, n_2}}{\partial y^2} \end{array} \right\} \quad (\text{C.4}) \\
&= -\frac{2}{\sqrt{3}} d^2 \sum_{n_1, n_2} \psi_{n_1, n_2}^* \left[\frac{3}{2} \left(\frac{\partial^2}{\partial x^2} + \frac{\partial^2}{\partial y^2} \right) - i3 \left(\mathbf{a}_x \frac{\partial}{\partial x} + \mathbf{a}_y \frac{\partial}{\partial y} \right) - |\mathbf{a}|^2 \right] \psi_{n_1, n_2} \\
&= -\int d^2 \mathbf{r} \psi_{n_1, n_2}^* \left[\nabla^2 - 2\mathbf{a} \cdot \nabla + \mathbf{a}^2 \right] \psi_{n_1, n_2}.
\end{aligned}$$

Note that A-B phases for unit vectors can be written as $\theta_{n_1, n_2}^1 = -\frac{\sqrt{3}}{4} b d^2 n_2 = -\frac{1}{2} b d \bar{y}$, $\theta_{n_1, n_2}^2 = \frac{b d}{4} (\sqrt{3} \bar{x} - \bar{y})$, $\theta_{n_1, n_2}^3 = \frac{b d}{4} (\sqrt{3} \bar{x} + \bar{y})$, therefore,

$$\begin{aligned}
(\theta_{n_1, n_2}^1)^2 + (\theta_{n_1, n_2}^2)^2 + (\theta_{n_1, n_2}^3)^2 &= \frac{3}{4} (d^2 b^2 x^2 + d^2 b^2 y^2) = d^2 \frac{3}{2} (\mathbf{a}_x^2 + \mathbf{a}_y^2) \quad (\text{C.5}) \\
2\theta_{n_1, n_2}^1 - \theta_{n_1, n_2}^2 + \theta_{n_1, n_2}^3 &= \frac{3}{2} b d \bar{y} = d 3 \mathbf{a}_x \\
\theta_{n_1, n_2}^2 + \theta_{n_1, n_2}^3 &= \frac{\sqrt{3}}{4} b d \bar{x} = \frac{d \sqrt{3}}{2} \mathbf{a}_y.
\end{aligned}$$

Put f_{grad} and f_{pot} together, It's clear that the formula for discretized free energy and continuum free energy are the same. Similarly, the discretized TDGL equation is the same as continuum TDGL equation.

For discretized free energy on rectangular grid, the potential term is nothing different, however, the gradient term has to modify. The gradient term for free energy is

$$\begin{aligned}
f_{\text{grad}} &= - \sum_{n_1, n_2=1}^{n_{\text{max}}} \psi_{n_1, n_2}^* \left\{ \left[\begin{array}{l} (U_{n_1, n_2}^1 \psi_{n_1+1, n_2} - \psi_{n_1, n_2}) + \\ \frac{4}{3} (U_{n_1, n_2}^2 \psi_{n_1, n_2+1} - \psi_{n_1, n_2}) + \end{array} \right] \right\} \quad (\text{C.6}) \\
&= - \sum_{n_1, n_2=1}^{n_{\text{max}}} \psi_{n_1, n_2}^* \left\{ \left[\begin{array}{l} \exp(-i\theta_{n_1, n_2}^1) \psi_{n_1+1, n_2} + \exp(i\theta_{n_1, n_2}^1) \psi_{n_1-1, n_2} + \\ \frac{4}{3} \exp(-i\theta_{n_1, n_2}^2) \psi_{n_1, n_2+1} + \frac{4}{3} \exp(i\theta_{n_1, n_2}^2) \psi_{n_1, n_2-1} + \\ -\frac{14}{3} \psi_{n_1, n_2} \end{array} \right] \right\}
\end{aligned}$$

Similarly as discretized free energy on hexagonal grid, both the link variables and order parameters are expand by using Taylor expansion.

$$\begin{aligned}
f_{\text{grad}} &= \sum_{n_1, n_2=1}^{n_{\text{max}}} \psi_{n_1, n_2}^* \left\{ \left[\begin{array}{c} \left(1 - i\theta_{n_1, n_2}^1 + \frac{(\theta_{n_1, n_2}^1)^2}{2} \right) \psi_{n_1+1, n_2} + \\ \left(1 + i\theta_{n_1, n_2}^1 + \frac{(\theta_{n_1, n_2}^1)^2}{2} \right) \psi_{n_1-1, n_2} + \\ \frac{4}{3} \left(1 - i\theta_{n_1, n_2}^2 + \frac{(\theta_{n_1, n_2}^2)^2}{2} \right) \psi_{n_1, n_2+1} + \\ \frac{4}{3} \left(1 + i\theta_{n_1, n_2}^2 + \frac{(\theta_{n_1, n_2}^2)^2}{2} \right) \psi_{n_1, n_2-1} + \\ -\frac{14}{3} \psi_{n_1, n_2} \end{array} \right] \right\} \quad (\text{C.7}) \\
&= \sum_{n_1, n_2=1}^{n_{\text{max}}} \psi_{n_1, n_2}^* \left\{ \begin{array}{c} \left[(\theta_{n_1, n_2}^1)^2 + (\theta_{n_1, n_2}^2)^2 \right] \psi_{n_1, n_2} + \\ -i2d \left[2\theta_{n_1, n_2}^1 \right] \frac{\partial \psi_{n_1, n_2}}{\partial x} + \\ -id \frac{4}{\sqrt{3}} \left[\theta_{n_1, n_2}^2 \right] \frac{\partial \psi_{n_1, n_2}}{\partial y} + \\ \frac{\partial^2 \psi_{n_1, n_2}}{\partial x^2} + \frac{\partial^2 \psi_{n_1, n_2}}{\partial y^2} \end{array} \right\} \\
&= -d^2 \sum_{n_1, n_2}^{n_{\text{max}}} \psi_{n_1, n_2}^* \left[\left(\frac{\partial^2}{\partial x^2} + \frac{\partial^2}{\partial y^2} \right) - i2 \left(\mathbf{a}_x \frac{\partial}{\partial x} + \mathbf{a}_y \frac{\partial}{\partial y} \right) - |\mathbf{a}|^2 \right] \psi_{n_1, n_2} \\
&= - \int d^2 \bar{\mathbf{r}} \psi_{n_1, n_2}^* \left[\nabla^2 - 2\mathbf{a} \cdot \nabla + \mathbf{a}^2 \right] \psi_{n_1, n_2}.
\end{aligned}$$

Note that A-B phases for unit vectors can be written as $\theta_{n_1, n_2}^1 = -\frac{\sqrt{3}}{4}bd^2n_2 = -\frac{1}{2}bdy$, $\theta_{n_1, n_2}^2 = \frac{\sqrt{3}}{4}bd^2n_1 = \frac{\sqrt{3}}{2}bdx$.

Appendix D

The Forward-Difference Method

Forward-Difference method is base on finite difference method which is one of the most popular method to solve partial differential equations with boundary conditions. Similar as finite difference method, discrete space part and replace the space derivative.

$$\frac{\partial^2 \psi}{\partial x^2}(x_i, t_j) = \frac{\psi(x_i + h, t_j) - 2\psi(x_i, t_j) + \psi(x_i - h, t_j)}{h^2} - \frac{h^2}{12} \frac{\partial^4 \psi}{\partial x^4}(\xi_i, t_j), \quad (\text{D.1})$$

where $\xi_i \in (x_{i-1}, x_{i+1})$. Similar as space, discrete time part and replace the time derivative.

$$\frac{\partial}{\partial t} \psi(x_i, t_j) = \frac{\psi(x_i, t_j + k) - \psi(x_i, t_j)}{k} - \frac{k}{2} \frac{\partial^2 \psi}{\partial t^2}(x_i, \mu_j), \quad (\text{D.2})$$

for some $\mu_j \in (t_j, t_{j+1})$. The local truncation error for this difference equation is

$$\tau_{ij} = \frac{k}{2} \frac{\partial^2 \psi}{\partial t^2}(x_i, \mu_j) - \frac{h^2}{12} \frac{\partial^4 \psi}{\partial x^4}(\xi_i, t_j). \quad (\text{D.3})$$

For linear diffusion equation, it's convenient to write equation represent as matrix, the system could implied as the tridiagonal form. For non-linear equation, it's difficult to calculate by matrix, thus, we solve equation of motion directly.